The Astrophysical Journal, 827:52 (34pp), 2016 August 10 doi:10.3847/0004-637X/827/1/52

A CENSUS OF YOUNG STARS AND BROWN DWARFS IN IC 348 AND NGC 1333*

K. L. Luhman[1,2], T. L. Esplin[1], and N. P. Loutrel[3]
[1] Department of Astronomy and Astrophysics, The Pennsylvania State University, University Park, PA 16802, USA; kluhman@astro.psu.edu
[2] Center for Exoplanets and Habitable Worlds, The Pennsylvania State University, University Park, PA 16802, USA
[3] Department of Physics, Montana State University, Bozeman, MT 59715, USA
Received 2016 March 8; revised 2016 May 2; accepted 2016 May 27; published 2016 August 5

ABSTRACT

We have obtained optical and near-infrared spectra of candidate members of the star-forming clusters IC 348 and NGC 1333. We classify 100 and 42 candidates as new members of the clusters, respectively, which brings the total numbers of known members to 478 and 203. We also have performed spectroscopy on a large majority of the previously known members of NGC 1333 in order to provide spectral classifications that are measured with the same scheme that has been applied to IC 348 in previous studies. The new census of members is nearly complete for $K_s < 16.8$ at $A_J < 1.5$ in IC 348 and for $K_s < 16.2$ at $A_J < 3$ in NGC 1333, which correspond to masses of $\gtrsim$0.01 $M_\odot$ for ages of 3 Myr according to theoretical evolutionary models. The faintest known members extend below these completeness limits and appear to have masses of ~0.005 $M_\odot$. In extinction-limited samples of cluster members, NGC 1333 exhibits a higher abundance of objects at lower masses than IC 348. It would be surprising if the initial mass functions of these clusters differ significantly given their similar stellar densities and formation environments. Instead, it is possible that average extinctions are lower for less massive members of star-forming clusters, in which case extinction-limited samples could be biased in favor of low-mass objects in the more heavily embedded clusters like NGC 1333. In the Hertzsprung–Russell diagram, the median sequences of IC 348 and NGC 1333 coincide with each other for the adopted distances of 300 and 235 pc, which would suggest that they have similar ages. However, NGC 1333 is widely believed to be younger than IC 348 based on its higher abundance of disks and protostars and its greater obscuration. Errors in the adopted distances may be responsible for this discrepancy.

Key words: brown dwarfs – protoplanetary disks – stars: formation – stars: low-mass – stars: luminosity function, mass function – stars: pre-main sequence

Supporting material: data behind figures, machine-readable tables

1. INTRODUCTION

A thorough census of young stars and brown dwarfs in nearby star-forming regions is important for measuring the global properties of young stellar populations (e.g., initial mass functions (IMFs), disk fractions) and for providing well-defined samples of targets for a variety of studies of star and planet formation. The Perseus molecular cloud is one of the nearest and richest of these regions (~300 pc, Schlafly et al. 2014). It contains several hundred young stars, most of which reside in two clusters, IC 348 and NGC 1333 (Herbst 2008; Walawender et al. 2008). Age estimates for IC 348 based on evolutionary models range from 2 to 6 Myr (Luhman et al. 2003b; Bell et al. 2013). NGC 1333 appears to be younger than IC 348 based on its greater obscuration and higher abundance of circumstellar disks and protostars (Muench et al. 2007; Gutermuth et al. 2008).

Candidate members of IC 348 have been identified via proper motions (Fredrick 1956; Scholz et al. 1999), Hα emission (Herbig 1954, 1998), X-ray emission (Preibisch et al. 1996; Preibisch & Zinnecker 2001, 2002, 2004; Forbrich et al. 2011; Stelzer et al. 2012), outflow signatures (Walawender et al. 2006; Hatchell & Dunham 2009), optical and near-infrared (IR) photometry (Strom et al. 1974b; Lada & Lada 1995; Luhman et al. 1998, 2003b; Luhman 1999; Najita et al. 2000; Mainzer & McLean 2003; Muench et al. 2003; Burgess et al. 2009; Alves de Oliveira et al. 2013), mid-IR excess emission (Jørgensen et al. 2006, 2007; Lada et al. 2006; Cieza et al. 2007; Muench et al. 2007; Rebull et al. 2007; Currie & Kenyon 2009; Evans et al. 2009; Young et al. 2015), variability (Flaherty et al. 2012, 2013; Cody & Hillenbrand 2014), and kinematics (Cottaar et al. 2015). Optical and near-IR spectroscopy has been used to measure spectral types and confirm membership for many of those candidates (Harris et al. 1954; Strom et al. 1974b; Herbig 1998; Luhman et al. 1998, 2003b, 2005b; Luhman 1999; Muench et al. 2007; Alves de Oliveira et al. 2013). Similar diagnostics of youth and membership have been applied to NGC 1333, including X-ray emission (Preibisch 1997, 2003; Getman et al. 2002; Winston et al. 2010; Forbrich et al. 2011), outflows (Hatchell & Dunham 2009), optical and near-IR photometry (Strom et al. 1976; Aspin et al. 1994; Lada et al. 1996; Aspin 2003; Wilking et al. 2004; Greissl et al. 2007; Oasa et al. 2008; Scholz et al. 2009), mid- IR excesses (Jørgensen et al. 2006, 2007; Cieza et al. 2007; Rebull et al. 2007; Gutermuth et al. 2008; Evans et al. 2009; Young et al. 2015), kinematics (Foster et al. 2015), and variability (Rebull et al. 2015). As in IC 348, spectroscopic classification has been performed on many of the resulting candidates (Aspin 2003; Wilking et al. 2004; Greissl et al. 2007; Scholz et al. 2009, 2012a, 2012b; Winston et al. 2009, 2010).

The current census of IC 348 is incomplete in the outer portions of the cluster and among the least massive brown dwarfs. The census of NGC 1333 has significant incompleteness as well, particularly at substellar masses. In addition, the

* Based on data from the NASA Infrared Telescope Facility, Gemini Observatory, Canada–France–Hawaii Telescope, Keck Observatory, Subaru Telescope, the Digitized Sky Survey, and the Two Micron All-Sky Survey.

Table 1
Members of IC 348

Column Label	Description
Name	Source name[a]
Luhman	Name from Luhman et al. (1998, 2003b, 2005b, 2005c), Luhman (1999), Muench et al. (2007), and this work
Evans	Name from Evans et al. (2009)
Stelzer	Name from Stelzer et al. (2012)
AlvesdeOliveira	Name from Alves de Oliveira et al. (2013)
OtherNames	Other source names
SpType	Spectral type
r_SpType	Spectral type reference[b]
Spectrograph	Spectrograph for spectral classification
Date	Date of spectroscopy
Adopt	Adopted spectral type
Aj	Extinction in J
IRexc	IR excess?[c]
pmRA	Relative proper motion in right ascension
e_pmRA	Error in pmRA
pmDec	Relative proper motion in declination
e_pmDec	Error in pmDec
Jmag	J magnitude
e_Jmag	Error in Jmag
Hmag	H magnitude
e_Hmag	Error in Hmag
Ksmag	K_s magnitude
e_Ksmag	Error in Ksmag
JHKref	JHK reference[d]

Notes.
[a] Coordinate-based identifications from the 2MASS Point Source Catalog when available. Otherwise, identifications are based on the coordinates measured from the WIRCam images in this work.
[b] (1) This work, (2) Muench et al. (2007), (3) Alves de Oliveira et al. (2013), (4) Luhman et al. (2003b), (5) Strom et al. (1974b), (6) Luhman et al. (1998), (7) Luhman (1999), (8) Harris et al. (1954), (9) Luhman et al. (2005b), (10) Herbig (1998), (11) Luhman et al. (2005c).
[c] Based on mid-IR photometry from the *Spitzer Space Telescope* (Luhman et al. 2005a; Lada et al. 2006; Muench et al. 2007; Currie & Kenyon 2009; Evans et al. 2009; Young et al. 2015).
[d] 2 = 2MASS Point Source Catalog; m = Muench et al. (2003); u = UKIDSS Data Release 10; w = WIRCam data from this work.

(This table is available in its entirety in machine-readable form.)

methods of spectral classification that have been applied to NGC 1333 are less uniform than in IC 348. To address these issues, we have performed a survey for new members down to ~0.005 $M_\odot$ across the full extent of each cluster, and we have measured spectral types for a large fraction of the known members of NGC 1333 with the classification scheme that we have previously applied to IC 348 and other nearby star-forming regions. In our presentation of this work, we begin by compiling lists of all known members of these clusters from previoius studies (Section 2). We then select candidate cluster members based on X-ray emission, mid-IR excess emission, optical and near-IR color–magnitude diagrams, and proper motions (Section 3) and use optical and near-IR spectra to measure their spectral types and determine whether they are members (Section 4). We also measure new spectral types for a large number of the known members of NGC 1333. We conclude by analyzing several aspects of the new samples of members of IC 348 and NGC 1333, which include their completeness, ages, mass functions, disk fractions, and spatial distributions (Section 5).

2. CENSUS FROM PREVIOUS STUDIES

We have searched previous studies of IC 348 and NGC 1333 for objects that exhibit evidence of membership. For IC 348, we began with the census of 288 members compiled by Luhman et al. (2003b). In that tabulation, pairs of objects with separations of $<1''$ appeared as single entries. We adopt the same approach in this work. Luhman et al. (2003b) noted that LRL 1434[4] was unusually faint for a cluster member near its spectral type, which would indicate that it is either a field star or a member that is detected in scattered light, as in the case of an edge-on disk. Because its Hα emission and Na I absorption in a low signal-to-noise ratio (S/N) spectrum seemed to indicate that it was young, Luhman et al. (2003b) adopted it as a member. However, it was not detected in subsequent mid-IR images of the cluster (Lada et al. 2006; Muench et al. 2007), indicating that it does not have a disk, and hence is unlikely to be seen in scattered light. Therefore, we omit LRL 1434 from our sample of members. In a low S/N spectrum from Luhman et al. (2003b), LRL 624 appeared to have the weak Na I absorption that is expected for a young, low-gravity cluster member. However, we now treat it as a field star based on its proper motion, which is inconsistent with membership in IC 348 (Section 3.5). Luhman et al. (2005c) measured spectral types for a likely companion in the census from Luhman et al. (2003b), LRL 78 B, and for the candidate companion LRL 166 B. Because LRL 166 B and its primary are separated by less than $1''$, they appear as a single entry in our tabulation of members. We have added to our sample the 16, 45, and 16 members identified by Luhman et al. (2005b), Muench et al. (2007), and Alves de Oliveira et al. (2013), respectively. The latter study presented spectra for several additional objects whose membership was uncertain. Based on our inspection of those spectra, we have classified five of those candidates as likely members (Section 4.2), consisting of sources 3, 5, 14, 20, and 31 from Alves de Oliveira et al. (2013; LRL 670, LRL 5209, LRL 10378, LRL 22443, LRL 54229). We include in our census the protostar HH 211-IR, the candidate protostellar brown dwarf IC 348-SMM2E (Palau et al. 2014), and LRL 1898, LRL 54361, LRL 54362, LRL 54419, LRL 54459, LRL 54460, LRL 55400, and LRL 57025 (Muench et al. 2007). The latter eight objects are probable protostars based on their spectral energy distributions and their proximity to millimeter cores and known protostars. Through the above steps, we arrived at a sample of 378 known members of IC 348 based on previous studies. Later in this work, we describe the identification of 100 new members, resulting in a total of 478 known members. We present the full sample of members in Table 1. The new members can be identified by the presence of a spectral type from this study alone with the exception of LRL 60 B and LRL 187 B. Although the latter stars lacked classifications prior to our spectroscopy, they are counted as previously known members rather than new ones since they appeared within the sample of members from Luhman et al. (2003b).

To construct a census of known members of NGC 1333, we assessed the evidence of membership for all objects proposed to be members in previous surveys of the cluster. The evidence consisted of signatures of youth in the form of strong emission

[4] When referring to objects in IC 348, we use the number identifications from our previous studies and from this work, which are found in the second column of Table 1.

lines, Li absorption, X-ray emission, mid-IR excess emission, and the shape of the gravity-sensitive steam bands. We also examined whether the proposed members exhibited radial velocities (Foster et al. 2015) and proper motions (Section 3.5) that are consistent with those of the larger population of objects that show evidence of youth. The radial velocity of 2MASS 03290289+3116010 and the proper motion of source 38 from Scholz et al. (2012b) indicate that they are unlikely to be cluster members. The previously reported members that we find have sufficient evidence of membership in NGC 1333 are listed in Table 2. We also include in that tabulation the new members found in our study. This census contains a total of 203 members. For 42 sources, our new spectral classifications are the only ones available, some of which were identified as candidate members in previous studies.

In our tabulations of members of IC 348 and NGC 1333, we have included all known young stars and brown dwarfs within the fields encompassed by the maps in Figure 1. However, one could argue that the objects at the largest distances from the centers of the clusters should instead be assigned to the distributed population that is present across the Perseus cloud (Young et al. 2015).

3. IDENTIFICATION OF CANDIDATE MEMBERS

To improve the completeness of the census of known members of IC 348 and NGC 1333, we have obtained spectra of candidate members that have been identified through several signatures of cluster membership. In this section, we describe the selection of these candidates.

3.1. Survey Fields

We have made use of several imaging surveys of IC 348 and NGC 1333 for identifying candidate members. In Figure 1, we show maps of the positions of the known members of the clusters and the boundaries of the fields in those surveys. IC 348 was observed with the imaging array of the Advanced CCD Imaging Spectrometer (ACIS-I) on the *Chandra* X-ray Observatory (Preibisch & Zinnecker 2001, 2002; Forbrich et al. 2011; Stelzer et al. 2012), CFH12K on the Canada–France–Hawaii Telescope (CFHT; *IZ*, Luhman et al. 2003b), and WIRCam and MegaCam on the CFHT ($z'JHK_s$, Alves de Oliveira et al. 2013). The MegaCam data encompass the entire field surrounding IC 348 in Figure 1. Data in *ZY JHK* are also available for all of IC 348 from Data Release 10 of the United Kingdom Infrared Telescope Infrared Deep Sky Survey (UKIDSS, Lawrence et al. 2007). NGC 1333 was observed with ACIS-I (Getman et al. 2002; Winston et al. 2010; Forbrich et al. 2011) and Suprime-Cam on Subaru Telescope ($i'z'$, Scholz et al. 2009). Unpublished images from WIRCam are also available for NGC 1333. We reduced all of the WIRCam images in JHK_s that are available for IC 348 and NGC 1333 from the CFHT archive, which were obtained through programs 07BH20 (K. Allers), 07BH12 (B. Biller), 09BD95 (L. Albert), O6BF23, 08BF98, and 09BF50 (J. Bouvier). The data from O6BF23 were those in IC 348 analyzed by Alves de Oliveira et al. (2013). We also reduced the Suprime-Cam images from Scholz et al. (2009), which were retrieved from the Subaru Telescope data archive.

Both clusters have been observed on many occasions at mid-IR wavelengths with the Infrared Array Camera (IRAC; Fazio et al. 2004) on the *Spitzer Space Telescope* (Werner et al. 2004). Through the c2d *Spitzer* Legacy project (Evans et al. 2003), shallow IRAC images were obtained for much of the Perseus cloud, including all of IC 348 and NGC 1333 (Jørgensen et al. 2006; Evans et al. 2009). Deeper images were taken for the larger IRAC fields indicated in Figure 1 (Lada et al. 2006; Muench et al. 2007; Gutermuth et al. 2008). The smaller IRAC fields in Figure 1 were monitored for approximately one month (Flaherty et al. 2013; Rebull

Table 2
Members of NGC 1333

Column Label	Description
Name	Source name[a]
Strom	Name from Strom et al. (1974a)
Aspin	Name from Aspin et al. (1994)
Lada	Name from Lada et al. (1996)
Getman	Name from Getman et al. (2002)
Wilking	Name from Wilking et al. (2004)
Gutermuth	Name from Gutermuth et al. (2008)
Oasa	Name from Oasa et al. (2008)
Evans	Name from Evans et al. (2009)
Scholz	Name from Scholz et al. (2009)
Winston	Name from Winston et al. (2010)
Rebull	Name from Rebull et al. (2015)
OtherNames	Other source names
SpType	Spectral type
r_SpType	Spectral type reference[b]
Spectrograph	Spectrograph for spectral classification
Date	Date of spectroscopy
Adopt	Adopted spectral type
Aj	Extinction in *J*
IRexc	IR excess?[c]
Evidence	Additional membership evidence[d]
pmRA	Relative proper motion in right ascension
e_pmRA	Error in pmRA
pmDec	Relative proper motion in declination
e_pmDec	Error in pmDec
Jmag	*J* magnitude
e_Jmag	Error in Jmag
Hmag	*H* magnitude
e_Hmag	Error in Hmag
Ksmag	K_s magnitude
e_Ksmag	Error in Ksmag
JHKref	JHK reference[e]

Notes.
[a] Coordinate-based identifications from the 2MASS Point Source Catalog when available. Otherwise, identifications are based on the coordinates measured from the WIRcam images in this work.
[b] (1) Winston et al. (2009), (2) this work, (3) Scholz et al. (2012b), (4) Scholz et al. (2009), (5) Cohen (1980), (6) Aspin (2003), (7) Wilking et al. (2004), (8) Greissl et al. (2007), (9) Scholz et al. (2012a), (10) Merin et al. (2010), (11) Connelley & Greene (2010), (12) Strom et al. (1974a), (13) Straižys et al. (2002), (14) Racine (1968), (15) Cieza et al. (2012).
[c] Based on mid-IR photometry and spectroscopy from the *Spitzer Space Telescope* (Gutermuth et al. 2008; Evans et al. 2009; Arnold et al. 2012; Rebull et al. 2015; Young et al. 2015).
[d] Membership in NGC 1333 is indicated by strong emission lines (e, Winston et al. 2009, 2010, this work), Li absorption (Li, Winston et al. 2009), X-ray emission (X, Getman et al. 2002; Winston et al. 2010; K. Getman 2016, in preparation), the shape of the gravity-sensitive steam bands (H_2O, Scholz et al. 2009, 2012b, 2012a, this work), or proper motions in Figure 4 (pm and pm?).
[e] 2 = 2MASS Point Source Catalog; *u* = UKIDSS Data Release 10; *w* = WIRCam data from this work.

(This table is available in its entirety in machine-readable form.)

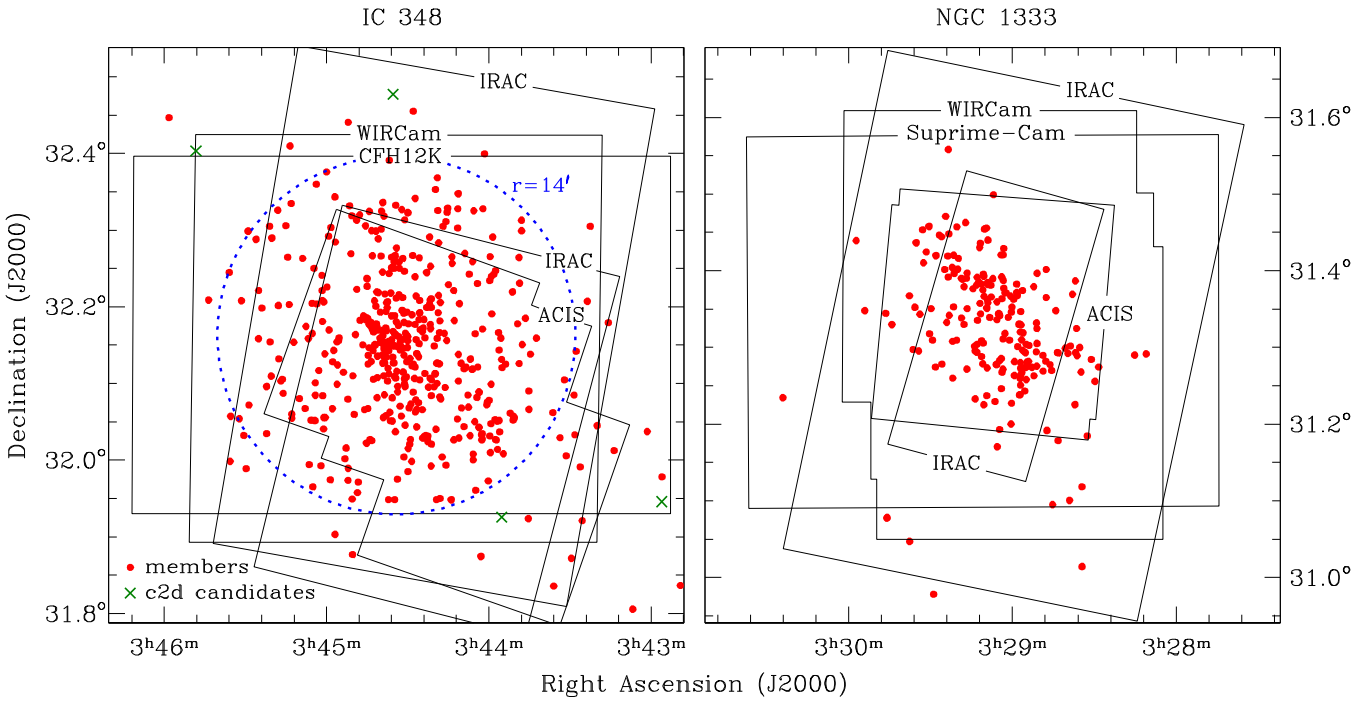

Figure 1. The positions of the known members of the IC 348 and NGC 1333 clusters (filled circles, Tables 1 and 2) and additional candidate young stars in the surrounding molecular cloud from the c2d survey (crosses, Evans et al. 2009; Young et al. 2015). We have marked the boundaries of fields that have been observed by ACIS-I on *Chandra* (Preibisch & Zinnecker 2001, 2002; Getman et al. 2002; Winston et al. 2010; Forbrich et al. 2011; Stelzer et al. 2012), IRAC on *Spitzer* (Lada et al. 2006; Muench et al. 2007; Gutermuth et al. 2008; Flaherty et al. 2013; Rebull et al. 2015), Suprime-Cam on Subaru (Scholz et al. 2009), and CFH12K and WIRCam on the CFHT (Luhman et al. 2003b; Alves de Oliveira et al. 2013, this work). MegaCam on the CFHT and UKIDSS imaged the entire field encompassed by the map of IC 348 (Alves de Oliveira et al. 2013). We have searched for new members of these clusters primarily within a radius of 14′ from the B5 star BD+31°643 in IC 348 (dotted circle) and within the ACIS-I field in NGC 1333.

et al. 2015). In the latest IRAC observations, most of each cluster was imaged at an additional epoch through program 90071 (A. Kraus) to facilitate the identification of candidate members via proper motions. The IRAC observations prior to 2009 May were performed with bands at 3.6, 4.5, 5.8, and 8.0 μm, denoted as [3.6], [4.5], [5.8], and [8.0], respectively. The later images were collected only in the [3.6] and [4.5] bands because of the depletion of the liquid helium coolant. The Multiband Imaging Photometer for *Spitzer* (MIPS; Rieke et al. 2004) also has been used to fully map each cluster at 24 μm (Lada et al. 2006; Rebull et al. 2007; Gutermuth et al. 2008; Currie & Kenyon 2009).

In addition to the known members and the survey fields, we also show in Figure 1 the positions of candidate disk-bearing stars that were identified by the c2d survey and that have not been observed with spectroscopy to confirm membership. Only a few of these candidates are present within the map of IC 348 and none are found in the map of NGC 1333, indicating that the distributions of known members trace the full extent of the clusters. The distribution for IC 348 has a radius of ∼14′, which is consistent with previous estimates of 10–15′ for the cluster radius (Scholz et al. 1999; Muench et al. 2003). We wish to achieve a census of the members of these clusters within fields that have well-defined boundaries, are large enough to encompass most of the members, and are small enough to be covered by as many imaging surveys as possible. Given these considerations, we have searched for new members primarily within a radius of 14′ from the B5 star BD+31°643 in IC 348 and within the 18′ × 18′ field in NGC 1333 that was observed by ACIS-I. We will assess the completeness of our new census within these fields in Section 5.1.

3.2. X-Ray Emission

Because young stars are bright in X-rays, one can search for members of star-forming regions via their X-ray emission (Feigelson et al. 1987; Walter et al. 1988). The X-ray studies of IC 348 and NGC 1333 (see Section 1) have done so by checking for X-ray sources that have optical and near-IR data that are consistent with those expected for cluster members. Most of the resulting candidate members have been observed with the spectroscopy that is needed to confirm membership. We have pursued spectroscopy of the remaining candidates that lack spectra. For this sample, we selected X-ray sources identified in *Chandra* images of IC 348 and NGC 1333 by Stelzer et al. (2012) and K. Getman (2016, in preparation), respectively, that are not rejected as non-members by our color–magnitude diagrams (Section 3.4). Those two studies have generated catalogs of sources found in all available ACIS-I images of the two clusters. In Table 1, the members of IC 348 that have X-ray detections can be identified by the presence of source names from Stelzer et al. (2012). For the members of NGC 1333, we indicate in Table 2 the X-ray detections from the new catalog of K. Getman under the column for membership evidence.

3.3. Mid-IR Excess Emission

When a star is born, it is surrounded by an accretion disk and an infalling envelope. The stars in a young cluster that still retain these structures can be identified via mid-IR emission in

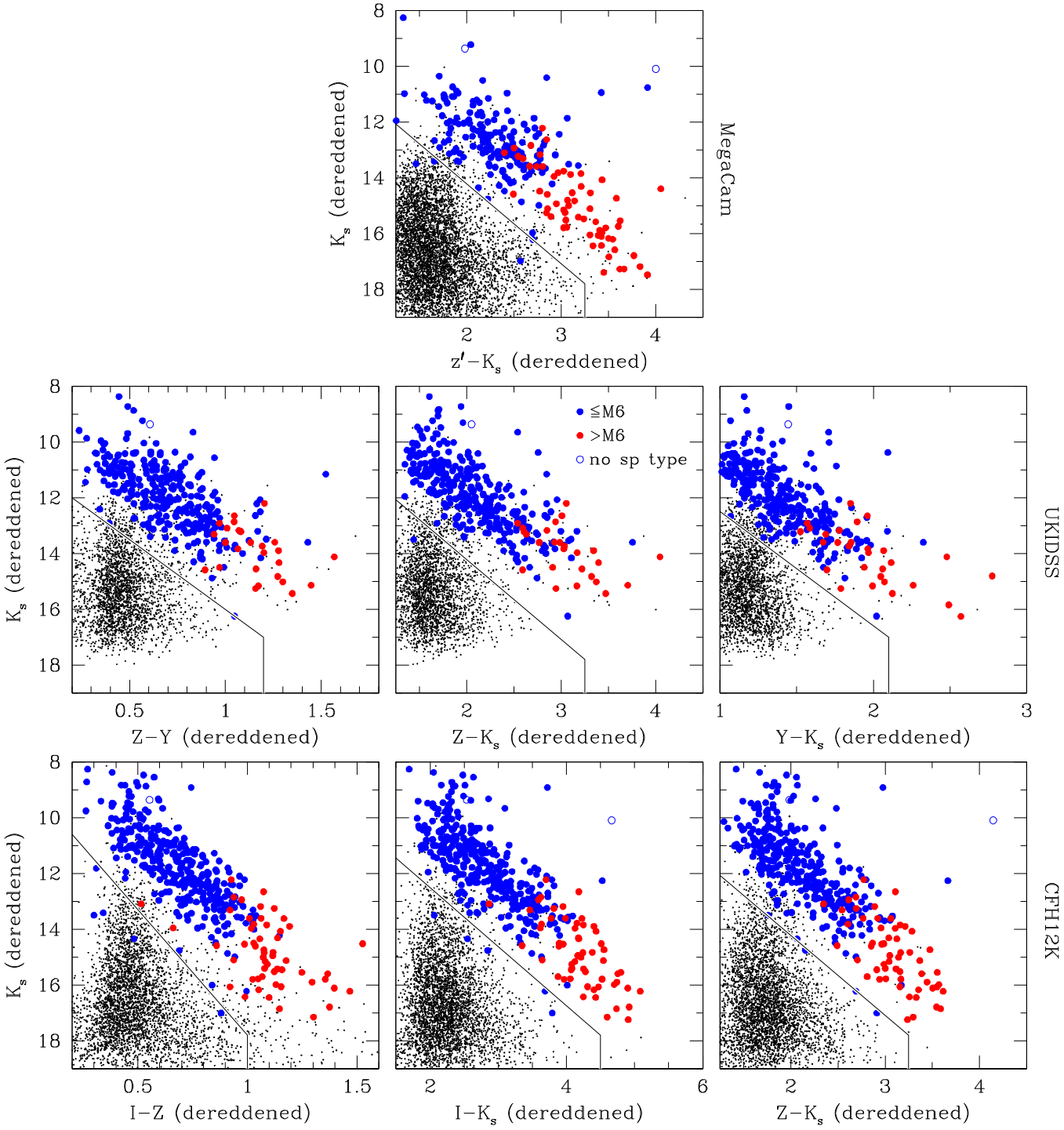

Figure 2. Extinction-corrected color–magnitude diagrams for the known members of IC 348 (large filled and open circles) and other sources (small points) within the area encompassed by the cluster map in Figure 1 (top and middle) and within the CFH12K field (bottom). These data are from MegaCam, UKIDSS, CFH12K, 2MASS, WIRCam, and Muench et al. (2003). Candidate members have been selected based on positions above the solid boundaries.

excess above that expected from a stellar photosphere. The *Spitzer* images described in Section 3.1 have been previously used to search for new members of IC 348 and NGC 1333 in that manner (Muench et al. 2007; Gutermuth et al. 2008; Evans et al. 2009; Young et al. 2015). As with the X-ray candidates, we have sought spectroscopy for the small fraction of mid-IR candidates that lack previous spectral classifications. When assembling this sample of candidates, we rejected those that appear to be knots of extended emission rather than stars based on visual inspection of the IRAC and MIPS images, which consist of sources 171, 216, 222, and 227 from Evans et al. (2009) and Young et al. (2015). If a young star is seen primarily in scattered light, as in the case of an edge-on disk, it is likely to appear unusually faint for its color compared to other cluster members. As a result, it would be prone to rejection as a field star in optical and near-IR color–magnitude diagrams. Therefore, we have retained mid-IR candidates in our spectroscopic sample regardless of their locations in the

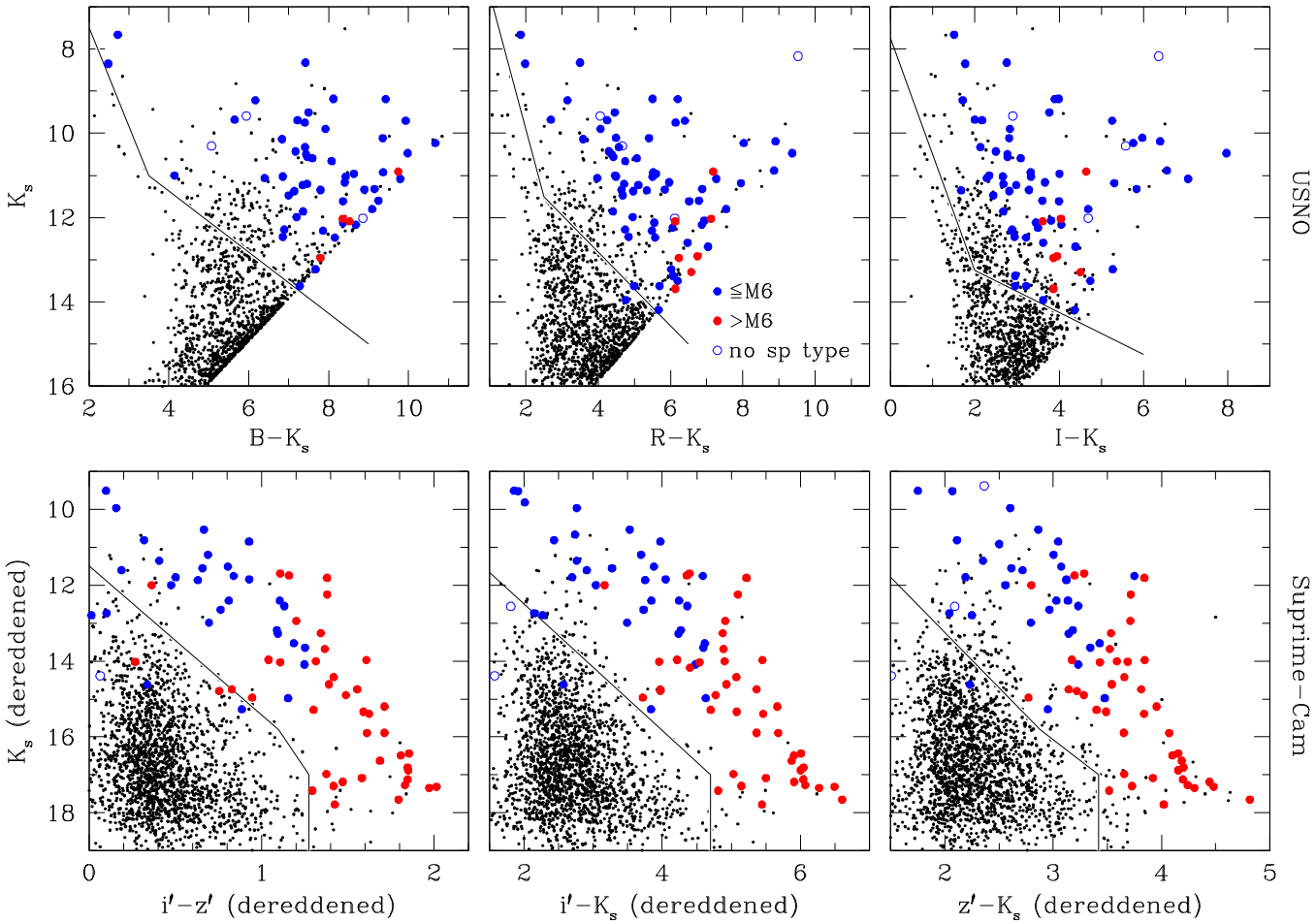

Figure 3. Color–magnitude diagrams for the known members of NGC 1333 (large filled and open circles) and other sources (small points) within the area encompassed by the cluster map in Figure 1 (top) and within the Suprime-Cam field (bottom). These data are from USNO-B1.0, Suprime-Cam, 2MASS, and WIRCam. Candidate members have been selected based on positions above the solid boundaries.

color–magnitude diagrams in Section 3.4. Active galactic nuclei and stars on the asymptotic giant branch are common types of contaminants in a sample of this kind that is selected via red mid-IR colors. The absence or presence of mid-IR excess emission is indicated for each known member of IC 348 and NGC 1333 in Tables 1 and 2, except for a few of the faintest members that lack sufficiently accurate mid-IR photometry.

3.4. Optical and Near-IR Color–Magnitude Diagrams

In the Hertzsprung–Russell (H–R) diagram, the members of a young, coeval stellar population appear along the main sequence at higher masses and diverge above the main sequence at lower masses, which is manifested in color–magnitude diagrams as a band that becomes redder at fainter magnitudes. For a nearby young cluster, that stellar sequence is brighter than most foreground and background stars. As a result, color–magnitude diagrams can be used to select a sample of candidate cluster members that has relatively little contamination from field stars.

To identify candidate members of IC 348, we have used the diagrams of I versus $R - I$ and m_{791} versus $m_{791} - m_{850}$ from Luhman (1999) and Luhman et al. (2005c), respectively. We also have constructed the following extinction-corrected diagrams: K_s versus $I - Z$, $I - K_s$, and $Z - K_s$ based on the I and Z data from Luhman et al. (2003b), K_s versus $Z - Y$, $Z - K_s$, and $Y - K_s$ based on the Z and Y data from UKIDSS, and K_s versus $Z - K_s$ based on the Z data that we have measured from MegaCam images. The K_s (or K) measurements are from the Point Source Catalog of the Two Micron All-Sky Survey (2MASS, Skrutskie et al. 2006), Muench et al. (2003), UKIDSS, and the WIRCam images described in Section 3.1. The extinctions of stars in these diagrams were estimated in the manner described by Luhman et al. (2003a) using the extinction law from Cardelli et al. (1989). In Figure 2, we show the extinction-corrected diagrams for the known members of IC 348 (including the new ones from this work) and all other sources with the exception of those that have been spectroscopically classified as field stars in this work and in previous studies. In each diagram, we have marked a boundary along the lower envelope of the locus of known members, which we have used for selecting candidate members for spectroscopy. The small number of known members that appear below the cluster sequence in some of the color–magnitude diagrams are likely seen in scattered light. They consist of LRL 435, LRL 725, LRL 904, LRL 1287, and LRL 4011. Luhman et al. (2003b) previously noted that LRL 435 and LRL 725 were unusually faint for their spectral types and colors.

For NGC 1333, we have constructed diagrams of K_s versus $B - K_s$, $R - K_s$, and $I - K_s$, where B, R, and I are photographic data from the USNO-B1.0 Catalog (Monet

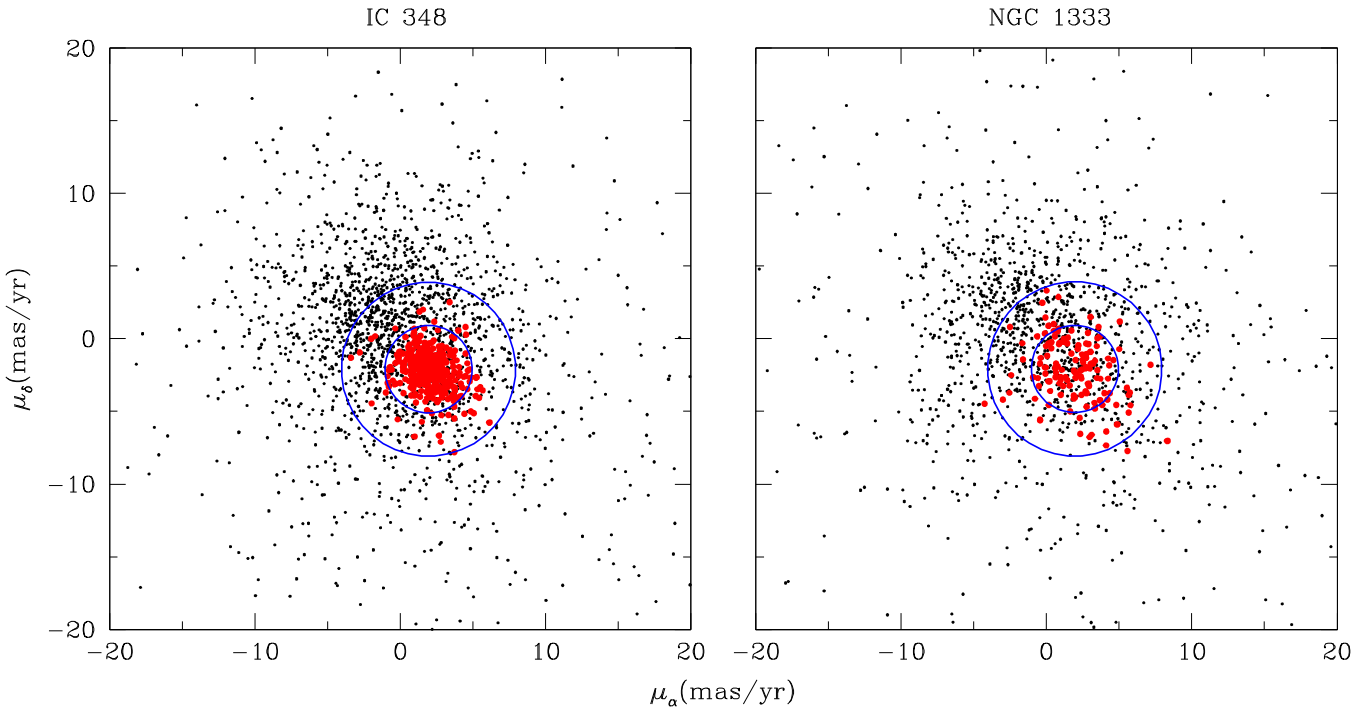

Figure 4. Relative proper motions for known members of IC 348 and NGC 1333 (large filled circles) and other sources detected in multi-epoch IRAC images (small points). When identifying candidate members of each cluster with photometry, we rejected objects with motions that differed by more than 6 mas yr^{-1} from the cluster medians (beyond outer circles). Photometric candidates that are within 3 and 3–6 mas yr^{-1} of the median motions (inner circle and outer annulus) are labeled as "pm" and "pm?" in Tables 4 and 5.

et al. 2003) and extinction-corrected diagrams of K_s versus $i' - z'$, $i' - K_s$, and $z' - K_s$ based on the i' and z' data from Suprime-Cam. The K_s data are from 2MASS, UKIDSS, and WIRCam. These diagrams are shown in Figure 3 for the known members of NGC 1333 and all other detected sources, excluding known field stars. As with IC 348, we have plotted a boundary that follows the lower envelope of the cluster sequence in each diagram for use in selecting candidate members. The known members that are below those boundaries consist of 2MASS J03291228+3123065 and sources 39, 66, 92, 102, 110, 113, and 122 from Gutermuth et al. (2008). All of these objects exhibit mid-IR excess emission, so it is plausible that they are seen in scattered light because of occulting disks.

For each cluster, a source is considered a candidate member if it is above a boundary in any diagram and is not below a boundary in any diagram. As an exception to the latter criterion, we do not reject candidates identified based on mid-IR excesses, as mentioned in the previous section.

3.5. Proper Motions

Nearby young clusters (150–300 pc) have proper motions of 10–20 mas yr^{-1}, and the members of a given cluster exhibit dispersions of $\sim$1 mas yr^{-1} ($\sim$1 km s^{-1}). In comparison, foreground and background stars typically have much larger and smaller motions, respectively. As a result, precise measurements of proper motions can be used to identify possible cluster members. To measure proper motions in IC 348 and NGC 1333, we have made use of the multiple epochs of IRAC observations that are available for the clusters, which were performed through programs 6 (G. Fazio), 36 (G. Fazio), 178 (N. Evans), 30516 (L. Looney), 50596 (G. Rieke), 60160 (J. Muzerolle), 61026 (J. Stauffer), 80174 (K. Flaherty), and 90071 (A. Kraus). We measured proper motions for all sources in these images by applying the astrometric techniques and distortion corrections from Esplin & Luhman (2016). Because the different epochs of astrometry have been registered using the stars that are in common among them (most of which are background stars), our analysis has produced relative proper motions. We have ignored proper motion measurements for sources with median values of S/N in the final epoch of exposures at 4.5 μm that are below 4 and 7.5 and that have errors larger than 6 and 8 mas yr^{-1} for IC 348 and NGC 1333, respectively. We were able to adopt a lower threshold of S/N for IC 348 because more epochs of IRAC images are available for it, which provides lower proper motion errors at a given S/N. We also inspected the IRAC images of the members that exhibited discrepant motions compared to the bulk of the population to identify and exclude measurements that were erroneous due to extended emission or blending of stars. Two previously identified members, LRL 624 in IC 348 and source 38 from Scholz et al. (2012b) in NGC 1333, appear to have reliable proper motion measurements that are inconsistent with membership, and hence have been rejected from the sample of members for each cluster, as mentioned in Section 2.

Among the 478 and 203 adopted members of IC 348 and NGC 1333, 405 and 141 sources (85 and 69%) have useful proper motions, respectively. A larger fraction of the stellar population in IC 348 has measured motions because of its greater number of IRAC epochs. The proper motions measured for known members are included in Tables 1 and 2. Those data have median values of (μ_α, $\mu_\delta = 1.9$, -2.1 mas yr^{-1}) for IC 348 and (μ_α, $\mu_\delta = 2.3$, -3.0 mas yr^{-1}) for NGC 1333. The motions for the known members and all other sources with measured motions are plotted in Figure 4. For each cluster, most of the members are within 3 mas yr^{-1} of the median value, and nearly all members are within 6 mas yr^{-1} of it.

Table 3
Field Stars in Spectroscopic Samples for IC 348 and NGC 1333

Name	Spectral Type	References[a]	Telescope/Instrument	Date
2MASS J03283231+3127079[b]	G–K	1	IRTF/SpeX	2015 Jan 6
2MASS J03283954+3121571[b]	<M0	1	IRTF/SpeX	2015 Jan 6
2MASS J03284197+3112171	<M3,<M0	2, 1	IRTF/SpeX	2015 Dec 14
2MASS J03284316+3126061[b]	<M3,F–K	2, 1	IRTF/SpeX	2015 Jan 7
2MASS J03284622+3112034	<M3,<K0	2, 1	IRTF/SpeX	2015 Dec 14
2MASS J03284624+3130120[b]	M3.5,<M3, M3.5	3, 2, 1	IRTF/SpeX	2013 Aug 27
2MASS J03284687+3120277[b]	M5V	1	IRTF/SpeX	2015 Jan 7
2MASS J03285521+3125223	<M3, G–K	2, 1	IRTF/SpeX	2015 Jan 6
2MASS J03285750+3113162[b]	giant	1	IRTF/SpeX	2015 Jan 8
2MASS J03290216+3116114[b]	M4.2, M, M3.5, M3.5	4, 5, 3, 1	IRTF/SpeX	2013 Aug 27
2MASS J03290862+3122297	<M0	1	IRTF/SpeX	2015 Dec 14
2MASS J03291793+3114535[b]	<M3, M1–M3:	2, 1	IRTF/SpeX	2015 Jan 7
2MASS J03291987+3118478[b]	<M3, F–K	2, 1	IRTF/SpeX	2015 Jan 8
2MASS J03292760+3121100	<M3, <M0	2, 1	IRTF/SpeX	2015 Jan 6
2MASS J03292805+3118391[b]	<M3, A–F	2, 1	IRTF/SpeX	2015 Jan 7
2MASS J03293084+3123529[b]	A–F	1	IRTF/SpeX	2015 Jan 6
2MASS J03293219+3117074[b]	<M3, A–F	2, 1	IRTF/SpeX	2015 Jan 6
2MASS J03293240+3113011[b]	F	1	IRTF/SpeX	2015 Jan 6
2MASS J03293441+3119106	G–K	1	IRTF/SpeX	2015 Jan 6
2MASS J03293476+3129081[b]	<M3, A–F	2, 1	IRTF/SpeX	2015 Jan 6
2MASS J03293654+3129465	giant	1	IRTF/SpeX	2015 Jan 6
2MASS J03293740+3117415[b]	<M3, F–G	2, 1	IRTF/SpeX	2015 Jan 6
2MASS J03293974+3114525	G–K	1	IRTF/SpeX	2015 Jan 6
2MASS J03293976+3121144[b]	G–K	1	IRTF/SpeX	2015 Jan 6
2MASS J03294283+3120147	B–A	1	IRTF/SpeX	2015 Jan 6
2MASS J03295048+3118305[b]	M3.0, M2.5	3, 1	IRTF/SpeX	2013 Aug 27
2MASS J03430722+3207169	early or giant	1	Magellan/IMACS	2005 Jan 4
2MASS J03430800+3201275	giant	1	Magellan/IMACS	2005 Jan 4
2MASS J03431143+3200276	early or giant	1	Magellan/IMACS	2005 Jan 4
2MASS J03431541+3211037	giant	1	Magellan/IMACS	2005 Jan 4
2MASS J03431928+3208537	giant	1	Magellan/IMACS	2005 Jan 4
2MASS J03433322+3213047	giant	1	Magellan/IMACS	2005 Jan 4
2MASS J03434503+3208479[b]	<M0	1	IRTF/SpeX	2011 Oct 4
2MASS J03434546+3201042	<M0	1	IRTF/SpeX	2015 Dec 14
2MASS J03434712+3213211	<M0	1	IRTF/SpeX	2015 Dec 14
2MASS J03435067+3213065[b]	<M0	1	IRTF/SpeX	2011 Oct 5
2MASS J03435160+3215565[b]	<M0	1	IRTF/SpeX	2011 Oct 4
2MASS J03435860+3218392	<M0	1	IRTF/SpeX	2011 Oct 4
2MASS J03440462+3220269[b]	giant	1	Magellan/IMACS	2005 Jan 4
2MASS J03440616+3220420	<M0	1	IRTF/SpeX	2011 Oct 4
2MASS J03440973+3217130	<M0	1	IRTF/SpeX	2011 Oct 4
2MASS J03441829+3218588[b]	<M0	1	IRTF/SpeX	2011 Oct 5
IC 348 IRS J03441847+3206421[b]	L	1	Gemini/GNIRS	2015 Jan 7
IC 348 IRS J03442070+3222489	<M0	1	IRTF/SpeX	2011 Oct 5
2MASS J03442086+3220439	<M0	1	IRTF/SpeX	2011 Oct 4
IC 348 IRS J03442188+3223370	<M0	1	IRTF/SpeX	2011 Oct 5
2MASS J03442250+3157054	M0-M2?	1	IRTF/SpeX	2015 Dec 14
IC 348 IRS J03442484+3213482	<M0	1	Gemini/GNIRS	2015 Nov 3
2MASS J03442761+3156369	<M0	1	IRTF/SpeX	2016 Jan 4
2MASS J03443036+3221528	<M0	1	IRTF/SpeX	2011 Oct 4
IC 348 IRS J03443089+3200154	<M0	1	Gemini/GNIRS	2015 Oct 25
2MASS J03443157+3157288	<K0	1	IRTF/SpeX	2016 Jan 4
2MASS J03443537+3156081	<M0	1	IRTF/SpeX	2011 Oct 5
2MASS J03443675+3220239	<M0	1	IRTF/SpeX	2011 Oct 5
2MASS J03444410+3158091	<M0	1	IRTF/SpeX	2015 Dec 14
2MASS J03444525+3156379	A	1	IRTF/SpeX	2011 Oct 4
2MASS J03444724+3156498[b]	<M0	1	IRTF/SpeX	2011 Dec 3
IC 348 IRS J03445102+3223094	<M0	1	IRTF/SpeX	2015 Dec 14
2MASS J03445462+3221405[b]	A	1	IRTF/SpeX	2011 Oct 4
IC 348 IRS J03445516+3212136	<M0	1	IRTF/SpeX	2015 Dec 14
2MASS J03450578+3159339	<M0	1	IRTF/SpeX	2011 Oct 5

Table 3
(Continued)

Name	Spectral Type	References[a]	Telescope/Instrument	Date
2MASS J03450980+3219303	<M0	1	IRTF/SpeX	2015 Dec 14
2MASS J03451154+3217358	<M0	1	IRTF/SpeX	2011 Oct 4
2MASS J03451566+3212090	<M0	1	IRTF/SpeX	2015 Dec 14
2MASS J03451737+3213591[b]	<M0	1	IRTF/SpeX	2011 Oct 4
2MASS J03451851+3206153[b]	<M0	1	IRTF/SpeX	2011 Oct 5
2MASS J03452158+3203289[b]	<M0	1	IRTF/SpeX	2011 Oct 5
2MASS J03452222+3203379	<M0	1	IRTF/SpeX	2015 Dec 14
2MASS J03452475+3209488	<M0	1	IRTF/SpeX	2015 Dec 14
2MASS J03452900+3203483	M3-M5	1	IRTF/SpeX	2016 Jan 4
2MASS J03452934+3200296[b]	<M0	1	IRTF/SpeX	2011 Oct 5
2MASS J03453078+3214320	M3.5 V	1	IRTF/SpeX	2011 Oct 5
2MASS J03453279+3208070	<M0	1	IRTF/SpeX	2011 Oct 4
2MASS J03453669+3213041	<M0	1	IRTF/SpeX	2011 Oct 5
2MASS J03453789+3208249	<M0	1	IRTF/SpeX	2011 Oct 4
2MASS J03453925+3210093	<G0	1	IRTF/SpeX	2011 Oct 4
2MASS J03453998+3208334	<M0	1	IRTF/SpeX	2015 Dec 14
2MASS J03454159+3214225	<M0	1	IRTF/SpeX	2011 Oct 4

Notes.
[a] (1) This work, (2) Scholz et al. (2012b), (3) Winston et al. (2009), (4) Wilking et al. (2004), (5) Scholz et al. (2009).
[b] Proper motion differs from cluster median by >6 mas yr^{-1} (outside of outer circle in Figure 4).

(This table is available in machine-readable form.)

Therefore, we consider objects within 6 mas yr^{-1} of the median motions to be candidates, and those within 3 mas yr^{-1} are the most promising ones. Sources with motions that differ by >6 mas yr^{-1} are rejected as non-members (although the previously known members that are only slightly beyond that threshold are retained as members). It is evident from Figure 4 that the known members overlap with a large number of field stars in their proper motion measurements. As a result, the sample of proper motion candidates has significant contamination from field stars, and it would be inefficient to pursue spectroscopy of candidates identified based on these measurements alone. However, these proper motions are valuable for refining the samples of candidates selected with the other methods that we have already described. If a candidate found with other diagnostics appeared to be a non-member based on its motion, we inspected its IRAC images prior to rejection to check for blends and extended emission that might lead to an erroneous proper motion measurement. Many of our spectra of candidates were obtained before we measured the IRAC proper motions. As a result, some of those objects in our spectroscopic sample would have been rejected by proper motions if they had been available, as indicated in Table 3.

4. SPECTROSCOPY

4.1. Observations

We have obtained spectra of 152 candidate members of IC 348 from the analysis in the previous section and 16 previously known members. We observed 130 sources with the near-IR spectrograph SpeX (Rayner et al. 2003) at the NASA Infrared Telescope Facility (IRTF). They consisted of 122 candidates (80 new members, 42 non-members) and eight known members. Three of the latter objects (LRL 464, LRL 659, LRL 10111) were candidates at the time of our spectroscopy and were independently identified as members by Alves de Oliveira et al. (2013). One known member in the SpeX sample (LRL 233) was placed in the slit during the observation of a candidate at a separation of 3″ (LRL 3171). The spectrum of the candidate was not useful because of low S/N, but we later successfully observed it with Gemini North. Another known member observed with SpeX (LRL 62) has a discrepant radial velocity relative to other cluster members (Cottaar et al. 2015), so we sought to verify the evidence of youth previously found through optical spectroscopy. The final three members observed with SpeX consist of the companions LRL 60 B and LRL 187 B, which lacked previous spectral classifications, and LRL 60 A. The SpeX data were collected in the prism mode with the 0.″8 slit (0.8–2.5 μm, $R = 150$). We performed optical spectroscopy on 15 candidates (8 new members, 7 non-members) and six known members (LRL 141, LRL 174, LRL 294, LRL 334, LRL 366, LRL 10094) with the Inamori Magellan Areal Camera and Spectrograph (IMACS) on the Magellan I telescope at Las Campanas Observatory. Those data were taken during the multi-slit observations described by Muench et al. (2007) for their sample of IR-selected candidates. The IMACS spectra spanned from 6300–8900 Å and exhibited a resolution of 3 Å. One of the known members observed with IMACS (LRL 10094) was originally selected as a candidate member and was subsequently classified as a member by Alves de Oliveira et al. (2013). We used the near-IR camera on the Keck I telescope (NIRC, Matthews & Soifer 1994) to obtain low-resolution (~100) spectra of one candidate (LRL 6005) and two known members from Luhman et al. (2005b) that had uncertain spectral types (LRL 1050, LRL 2103). They were observed with the gr120 and gr150 grisms, which together provided coverage from 1–2.5 μm. We observed two and 12 candidates with the Gemini Near-Infrared Imager (NIRI, Hodapp et al. 2003) and the Gemini Near-Infrared Spectrograph (GNIRS, Elias et al. 2006), respectively, at the Gemini North telescope. NIRI was operated with the H-band grism and the 0.″75 slit ($R = 500$). The GNIRS data were collected in the

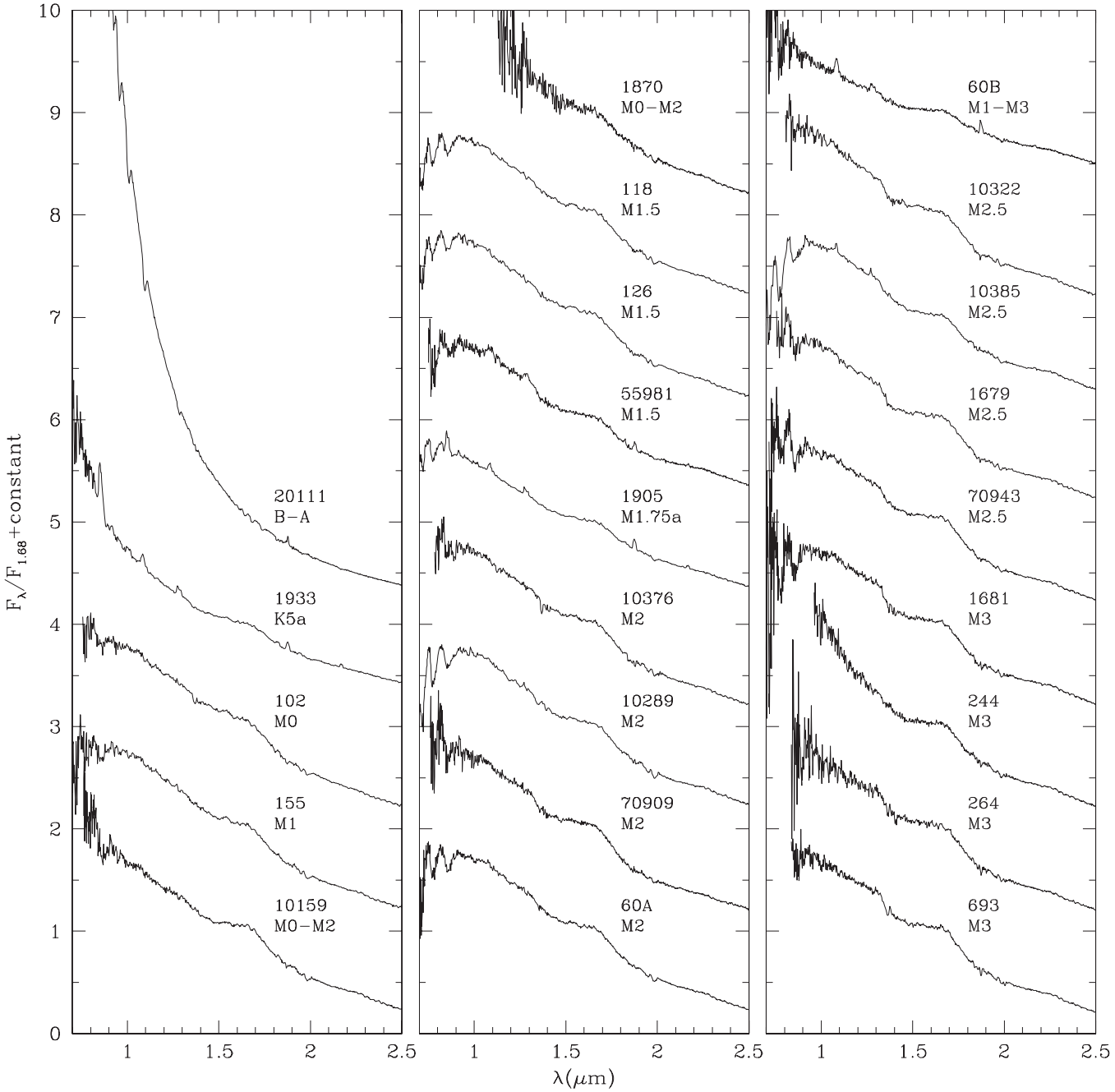

Figure 5. Near-IR spectra of members of IC 348 from this work and Muench et al. (2007). The spectral types denoted with "a" have been adopted from optical spectra because accurate types could not be measured from these IR data (LRL 1933, LRL 1905) or the objects serve as standards for classifying our IR spectra (LRL 147, LRL 201, LRL 405). The remaining types have been measured from these spectra. The spectra have been dereddened to match the slopes of standards near 1 μm. These data have a resolution of $R = 150$.

(The data used to create this figure are available.)

cross-dispersed mode with the 31.7 l mm^{-1} grating and the 0.″67 slit (1–2.5 μm, $R = 800$). The 152 candidates observed by these spectrographs consist of 100 new members and 52 non-members based on the classifications from the next section.

In NGC 1333, we have performed spectroscopy on 55 candidate members and 124 known members with SpeX and 14 candidates with GNIRS. The instrument configurations were the same as those employed for the targets in IC 348 except for BD+30°547, for which we used the SXD mode of SpeX with the 0.″8 slit (0.7–2.5 μm, $R = 750$) because its earlier type required higher resolution for classification. We included a large number of known members in our spectroscopic sample because we wish to maximize the number of members that are classified in the same manner as the members of IC 348. In the next section, we find that 42 and 26 candidates are members and non-members, respectively, and that one of the candidates (J03284883+3117537) has an uncertain classification because of low S/N.

The SpeX data were reduced with the Spextool package (Cushing et al. 2004) and corrected for telluric absorption in the

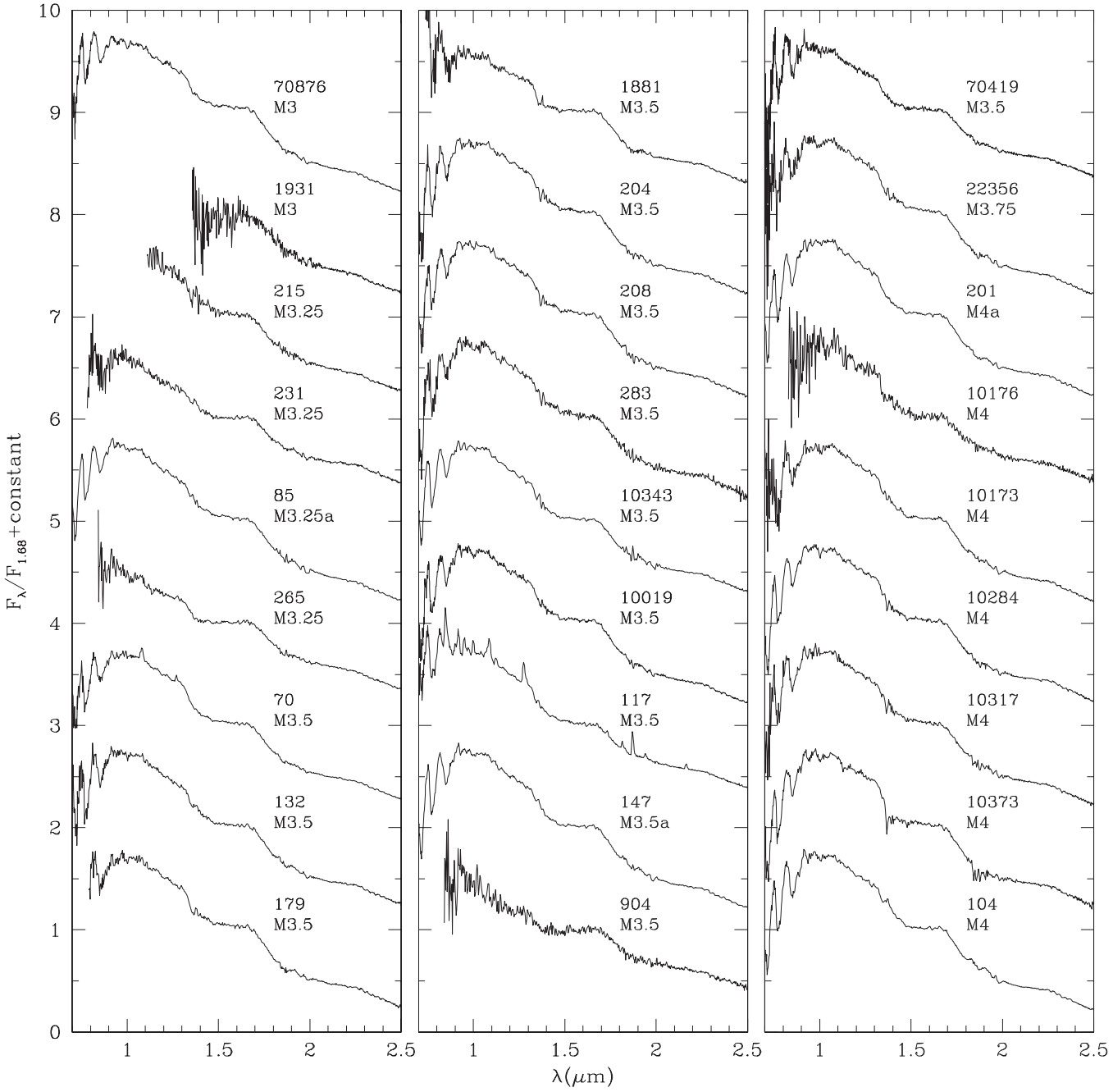

Figure 6. More near-IR spectra of members of IC 348 (see Figure 5).
(The data used to create this figure are available.)

manner described by Vacca et al. (2003). For the IMACS and NIRC spectra, we used routines within IRAF to apply bias subtraction and flat fielding to the two-dimensional images, extract spectra of the targets from those images, and perform wavelength calibration on the extracted data with spectra of arc lamps. Each NIRC spectrum was also corrected for telluric absorption using the spectrum of an A star that was observed at a similar airmass.

The dereddened near-IR spectra of the new members of IC 348 and NGC 1333 are presented in Figures 5–10 and Figures 11–17, respectively. We also include all of our SpeX data for previously known members from this work and previous studies (Luhman et al. 2005c; Muench et al. 2007) with the exception of the four featureless spectra in IC 348 that were presented by Muench et al. (2007). Within the lists of all known members of the clusters in Tables 1 and 2, we indicate the dates and instruments for our new spectra and the previous SpeX data. The candidates from our spectroscopic sample that we have classified as non-members are found in Table 3.

4.2. Spectral Classification

We have used the spectra that we have collected to measure spectral types of our targets and to help determine whether they

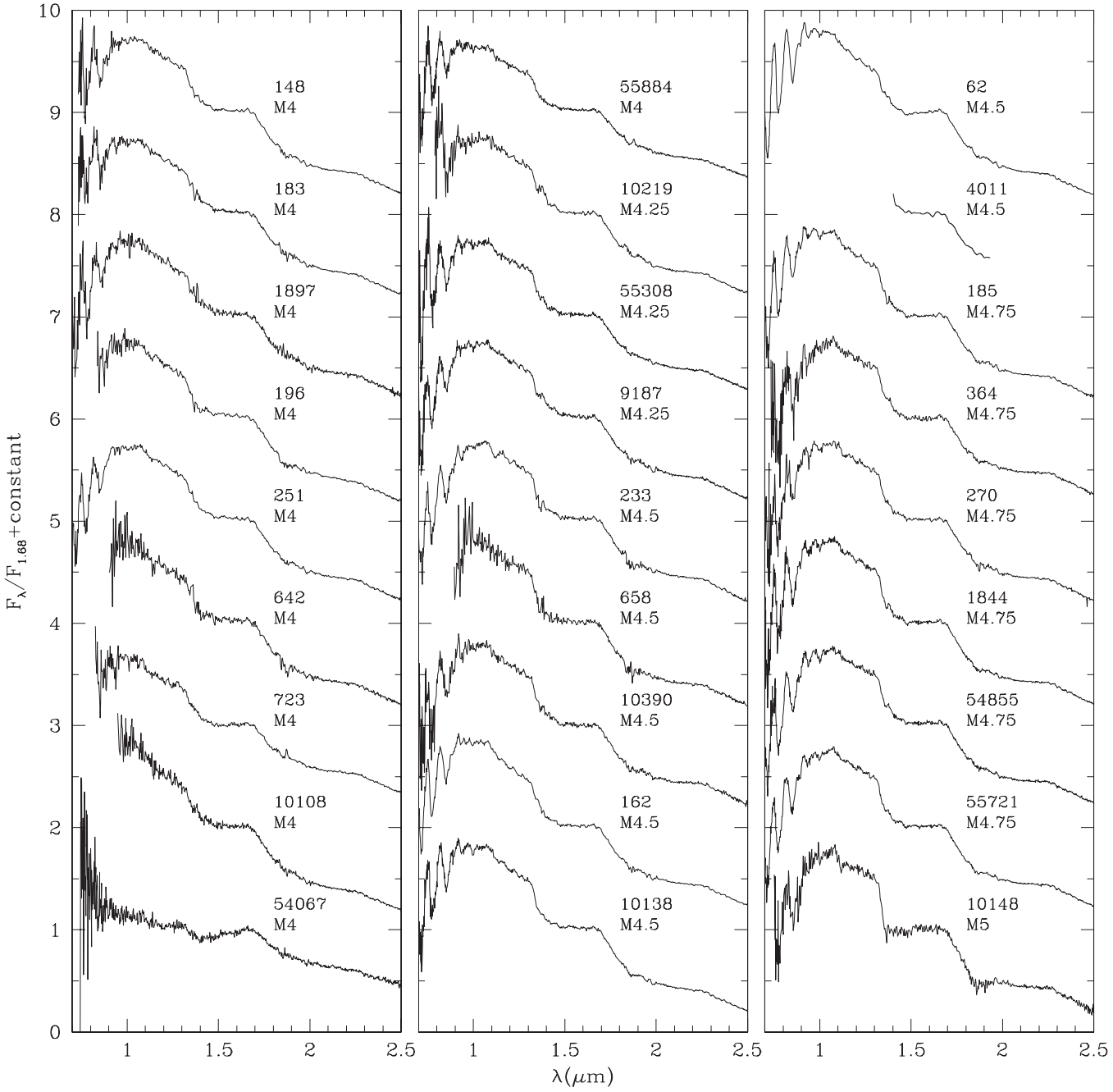

Figure 7. More near-IR spectra of members of IC 348 (see Figure 5).
(The data used to create this figure are available.)

are members of IC 348 and NGC 1333. Seven of our targets of optical spectroscopy lack the M-type spectral features (TiO, VO) expected if they were members of IC 348, indicating that they are likely early-type field stars or giants that are behind the cluster. The remaining 14 objects with optical spectra do exhibit M-type features, all of which are young based on their Na I and K I absorption lines, which are sensitive to surface gravity. We measured spectral types from these data through comparison to the averages of dwarf and giant standards (Luhman 1999). In previous studies (e.g., Muench et al. 2007), we have measured spectral types from near-IR spectra of young late-type objects via comparison to spectra of individual young late-type objects that we had classified at optical wavelengths. Because of the relatively large number of young objects that now have both optical types and near-IR spectra, we have recently combined the spectra of several such objects for each subclass (K. Luhman 2016, in preparation). We have used the resulting spectra as standards for classifying the near-IR spectra in IC 348 and NGC 1333 that exhibit steam absorption ($\gtrsim$M0) and evidence of youth (e.g., triangular *H*-band continuum Lucas et al. 2001). For the remaining IR data, spectral types were measured with spectra of standard dwarfs and giants from our previous studies and from Cushing et al. (2005) and Rayner et al. (2009). In addition, we have revised our previous

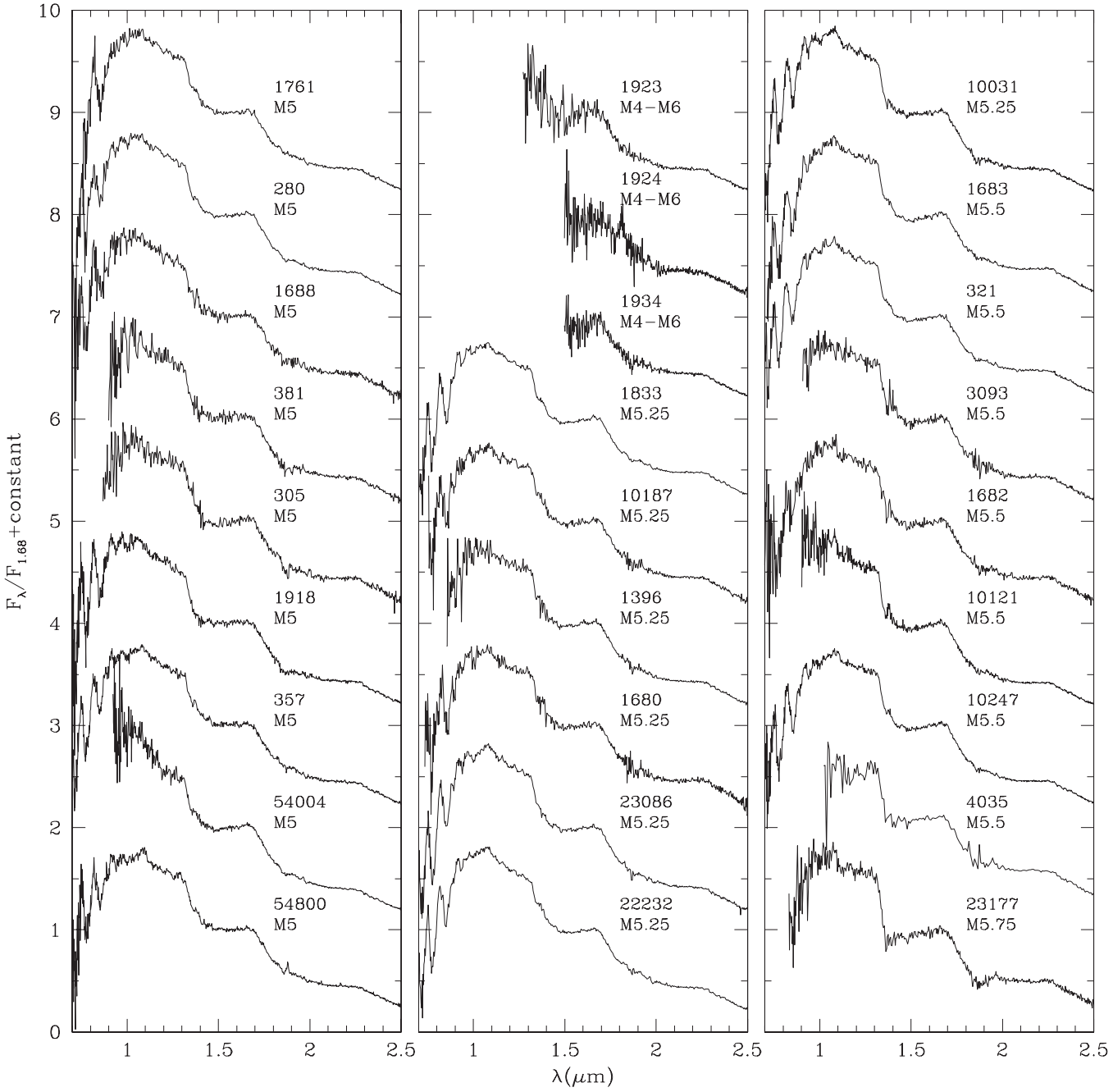

Figure 8. More near-IR spectra of members of IC 348 (see Figure 5).
(The data used to create this figure are available.)

classifications of SpeX data for members of IC 348 (Luhman et al. 2005c; Muench et al. 2007) using the new standard spectra. The resulting changes are $\leqslant$0.25 subclass for most objects. We also measured spectral types from the near-IR spectra of candidate members of IC 348 presented by Alves de Oliveira et al. (2013). For one of those objects, LRL 5209, the S/N appeared to be lower than expected for its magnitude, so we performed our own reduction of the raw data. We have included the new version of the spectrum with the data that we have collected in Figure 10. Most of our classifications are similar to those from Alves de Oliveira et al. (2013). For those cases, we adopt the types from Alves de Oliveira et al. (2013). We do present our new spectral types for LRL 670, LRL 5209, and LRL 22443 since they differ noticeably from the previous measurements. In addition, whereas Alves de Oliveira et al. (2013) classified the membership status of LRL 670, LRL 5209, LRL 10378, LRL 22443, and LRL 54229 as uncertain, we find that the spectra of these objects from Alves de Oliveira et al. (2013) do show sufficient evidence of membership in the form of the gravity sensitive features. As a result, we have included those objects in our census of members, as mentioned in Section 2.

For the members of IC 348 and NGC 1333 that have measured spectral types and that have SpeX data from this

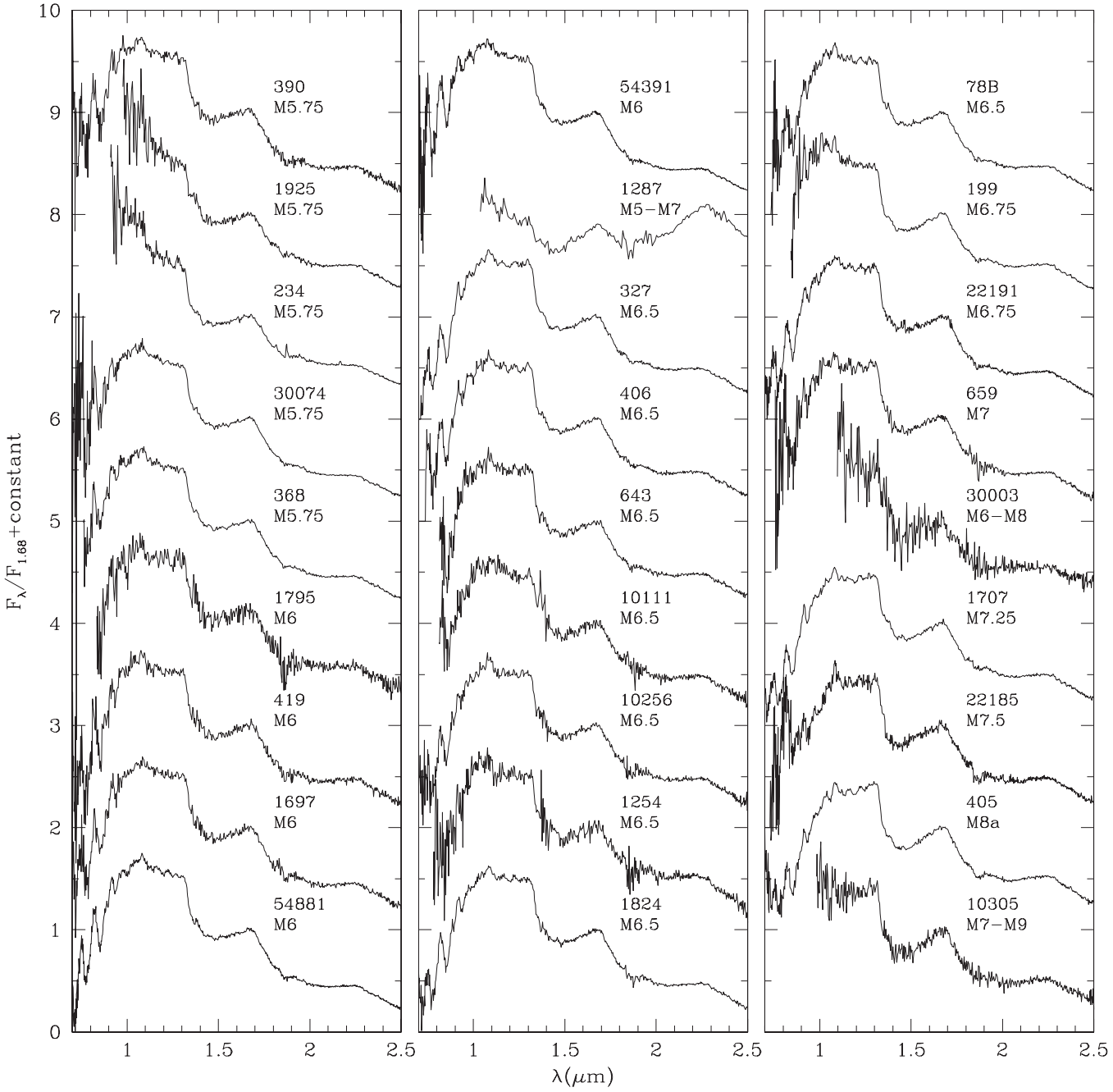

Figure 9. More near-IR spectra of members of IC 348 (see Figure 5).
(The data used to create this figure are available.)

work and our previous studies, we have estimated extinctions by comparing the observed spectral slopes at 1 μm to the slopes our young standards and adopting the extinction law of Cardelli et al. (1989). If a spectral type could not be measured from a SpeX spectrum, but a classification was available from another source (e.g., optical spectrum), then we adopted that classification when estimating the extinction. For a spectrum with low S/N at 1 μm, we estimated the extinction from the slope at longer wavelengths if a *K*-band excess was unlikely to be present based on an absence of a mid-IR excess. The resulting extinctions were used for dereddening the spectra in Figures 5–17. Among those dereddened spectra, most of the objects with high extinctions can be identified by their lower S/N at shorter wavelengths.

The spectral types that we have measured for members of IC 348 and NGC 1333 are included within the lists of all known members in Tables 1 and 2. The errors for the optical and IR types are $\pm$0.25 and 0.5 subclass, respectively, unless indicated otherwise. The uncertainties in the IR types tend to be large at $\gtrsim$M9 because of a degeneracy between spectral type and reddening in near-IR spectra with low resolution and low-to-moderate S/N. For instance, a young M9 object with $A_V \sim 3.5$ can appear quite similar to an unreddened L3 object in data of this kind. Our classifications for non-members are

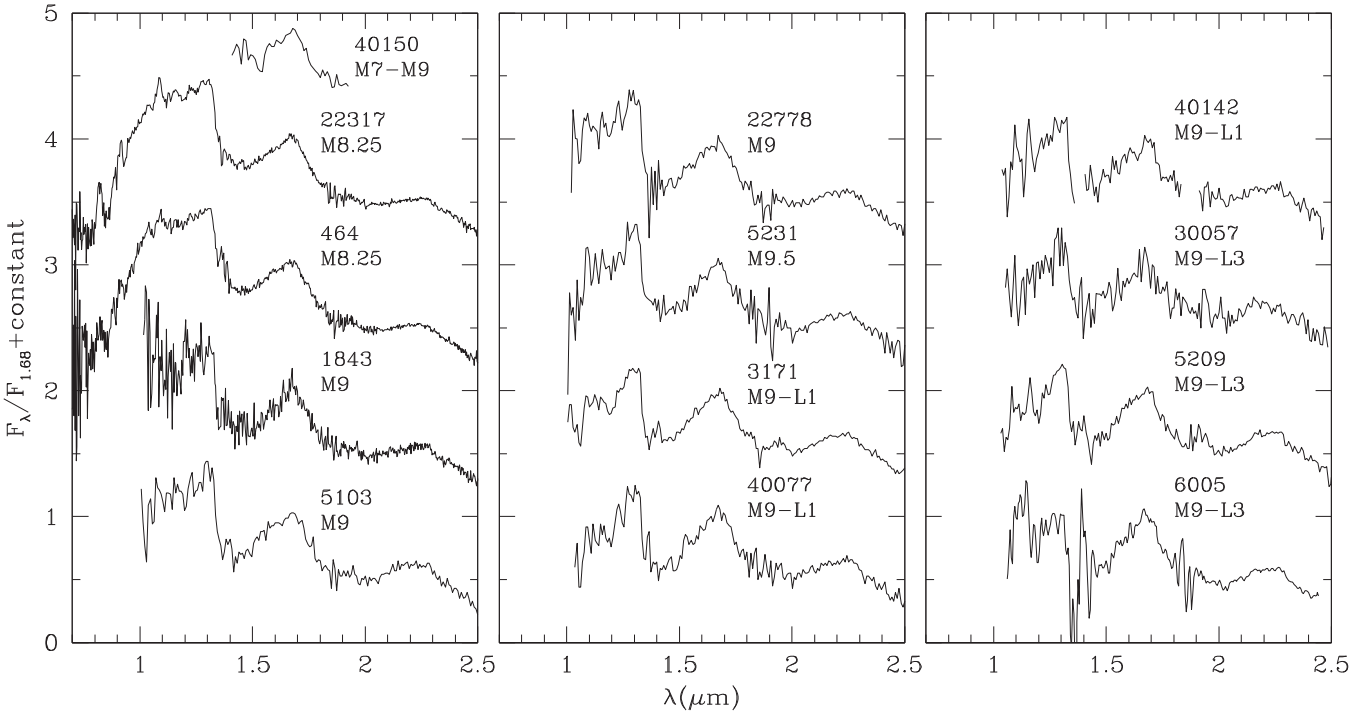

Figure 10. More near-IR spectra of members of IC 348 (see Figure 5).
(The data used to create this figure are available.)

presented in Table 3. Most of these non-members are giants and early-type stars, which are difficult to distinguish from K and early-M cluster members in color–magnitude diagrams. Meanwhile, cooler members have more distinctive colors, so the yield of confirmed members can be higher at fainter magnitudes when the appropriate bands of photometry are available. For instance, 13 of the 14 candidate low-mass members of NGC 1333 observed with GNIRS were confirmed as such. Finally, we note that several of the candidate members of IC 348 that we selected from our color–magnitude diagrams and confirmed with spectroscopy were previously identified as photometric candidates by Alves de Oliveira et al. (2013), consisting of LRL 6005, LRL 5231, LRL 1254, LRL 1824, and LRL 22778.

4.3. Comparison to Previous Work

We have compared our membership lists and spectral types for IC 348 and NGC 1333 to those from previous studies. We have presented spectra for 100 and 42 members of these clusters, respectively, that have not been previously classified, which we refer to as new members. Two additional stars, LRL 60 B and LRL 187 B, also lack previous classifications, but they are treated as previously known members, as mentioned in Section 2. To illustrate the magnitudes and spectral types at which the census of these clusters has expanded, we show in Figure 18 the distributions of extinction-corrected M_K and spectral types for previously known and new members. We have adopted the extinctions estimated from our IR spectra in Section 4.2 when available. Otherwise, extinctions are estimated with photometry in the manner described in Section 5.2. Members that lack measured spectral types (and hence extinctions) are absent from Figure 18, which consist of protostars with featureless spectra. The new members of IC 348 are predominantly low-mass stars at M4–M6 in the outskirts of the cluster, but they also include several objects that are the faintest known members. In NGC 1333, the new members are distributed more uniformly with magnitude and spectral type among the low-mass stars and brown dwarfs.

Rebull et al. (2015) compiled a sample of 130 members of NGC 1333, 17 of which are absent from our census of the cluster for the following reasons. Seven of these missing objects are among the candidate members that we have identified in Section 3, but they lack spectroscopic confirmation of their membership. They consist of 2MASS J03291532+3129346 and NGC 1333 IRS J03284883+3117537, J03285358+3112147, J03285508+3114163, J03291565+311911, J03285709+3121250, and J03291317+3119495. Sources 12, 45, 113, and 174 from Winston et al. (2010) have been detected in X-rays, but are rejected as field stars by our color–magnitude diagrams and have no other evidence of membership. Using the identifiers from Gutermuth et al. (2008), sources 38 and 76 are field stars based on our spectroscopy, sources 8 and 38 are an outflow lobe and a galaxy, respectively (Arnold et al. 2012), source 95 has uncertain membership (Section 4.4), and source 26 is extended at both near- and mid-IR wavelengths, so it is unclear whether it a star.

Rebull et al. (2015) identified five new candidate members of NGC 1333 based on their mid-IR variability. One of these candidates, SSTYSV J032903.46+311617.9, is in our spectroscopic sample. Based on its featureless near-IR spectrum and red color in [3.6]–[4.5] (it is blended with a brighter star at longer wavelengths), it is probably a protostar, so we have included it in our census of members. Rebull et al. (2015)

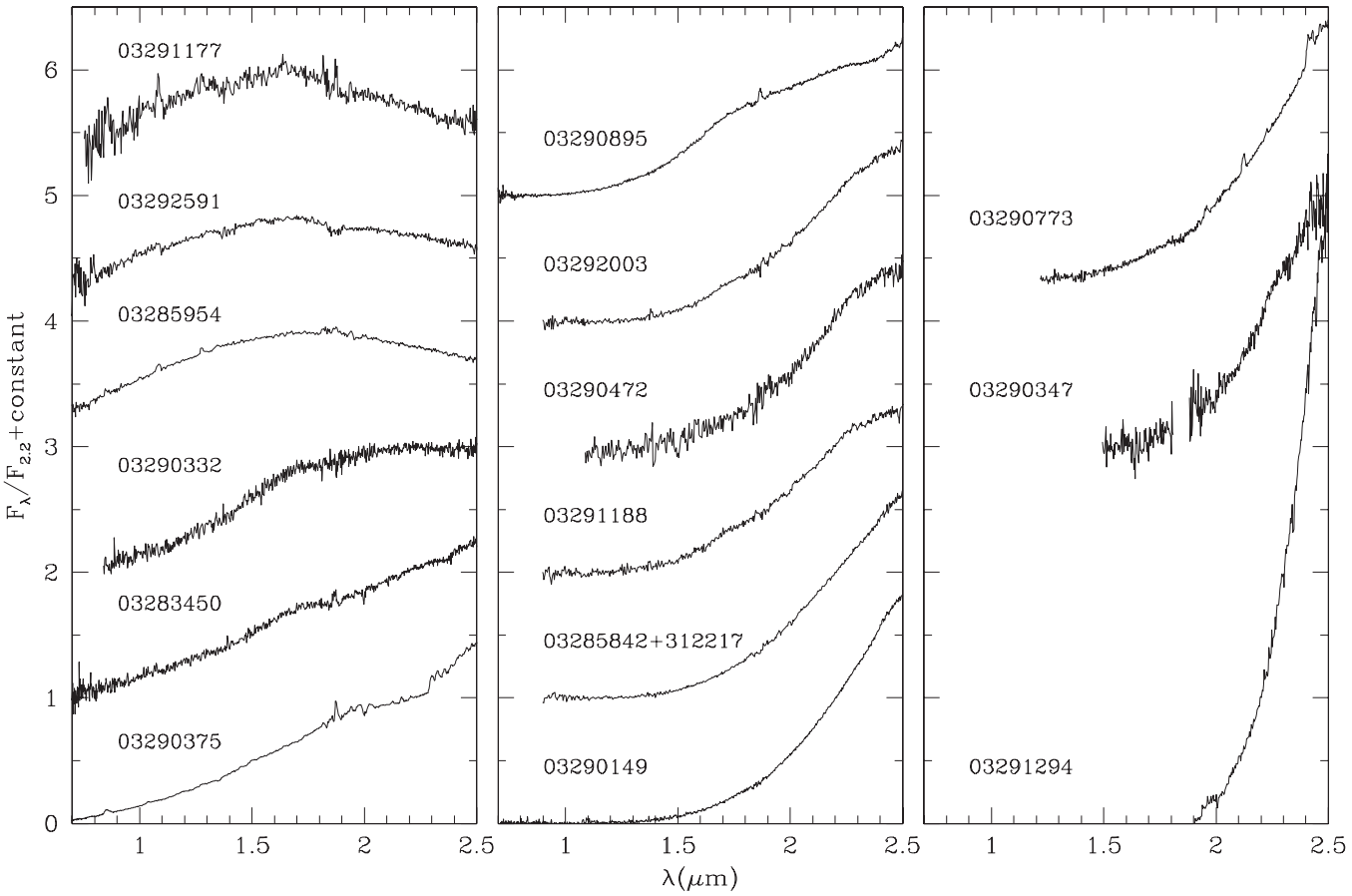

Figure 11. Near-IR spectra of members of NGC 1333 that lack measured spectral types because photospheric absorption features were not detected (e.g., protostars). These data have a resolution of $R = 150$. Each spectrum is labeled with the portion of the source name from Table 2 that corresponds to R.A. For one object, additional digits of decl. are listed to uniquely identify it among the members.

(The data used to create this figure are available.)

discussed at length a second of their candidates, SSTYSV J032911.86+312155.7. They classified it as a possible protostar based on its flux at 24 μm relative to shorter wavelengths. However, we find that no detection is apparent in the 24 μm images. Bright extended emission associated with the nearby star SVS 3 prevents detections in the *Spitzer* bands longward of 4.5 μm. Nevertheless, given its close proximity to other members like SVS 3 and the excess at 4.5 μm relative to bands at shorter wavelengths, it is a promising candidate member. We include it in our list of candidates that have not been observed with spectroscopy in Section 5.1. Two other objects from Rebull et al. (2015), SSTYSV J032918.65 +312021.8 and SSTYSV J032907.24+312409.7, are also in our sample of candidates based on their variability, mid-IR excess emission, and their positions in our color–magnitude diagrams. The final candidate from Rebull et al. (2015), SSTYSV J032836.43+312856.7, does not exhibit mid-IR excess emission and is rejected by our color–magnitude diagrams, so we do not consider it to be a candidate member.

As mentioned in Section 4.1, we have performed spectroscopy on a large number of the previously known members of NGC 1333 with the goal of obtaining spectral classifications that are derived with the same scheme applied to IC 348 in our previous studies and this work. Spectral types are available from both our work and previous studies for 90 objects. For a majority of the previous classifications, there is not a systematic difference from our measurements. However, we do find that our spectral types are an average of ∼1 subclass earlier than those from Scholz et al. (2009, 2012a, 2012b), which corresponds to ∼50% higher mass estimates when combined with evolutionary models (e.g., Baraffe et al. 1998). There remain several (very faint) members from Scholz et al. (2009, 2012a, 2012b) for which we have not obtained spectra and measured spectral types.

4.4. Comments on Individual Sources

LRL 62 and LRL 155. The optical spectrum of LRL 62 from Luhman (1999) exhibits a spectral type of M4.5 and evidence of youth in the form of weak K I and Na I lines. However, its radial velocity of ∼5 km s^{-1} differs significantly from the mean value of 15.4 km s^{-1} ($\sigma = 0.7$ km s^{-1}) for a sample of known members (Cottaar et al. 2015). We obtained a near-IR spectrum to verify its youth through additional gravity-sensitive features. Our new classification based on that spectrum is consistent with the optical result. Like LRL 62, LRL 155 also has a discrepant radial velocity (∼23 km s^{-1}). Its near-IR spectrum indicates a spectral type of M1, but it is not sensitive to signatures of low surface gravity for this type. Both stars have higher extinctions ($A_J = 0.7$ and 1) than expected for foreground dwarfs ($A_J < 0.1$) and are too bright for

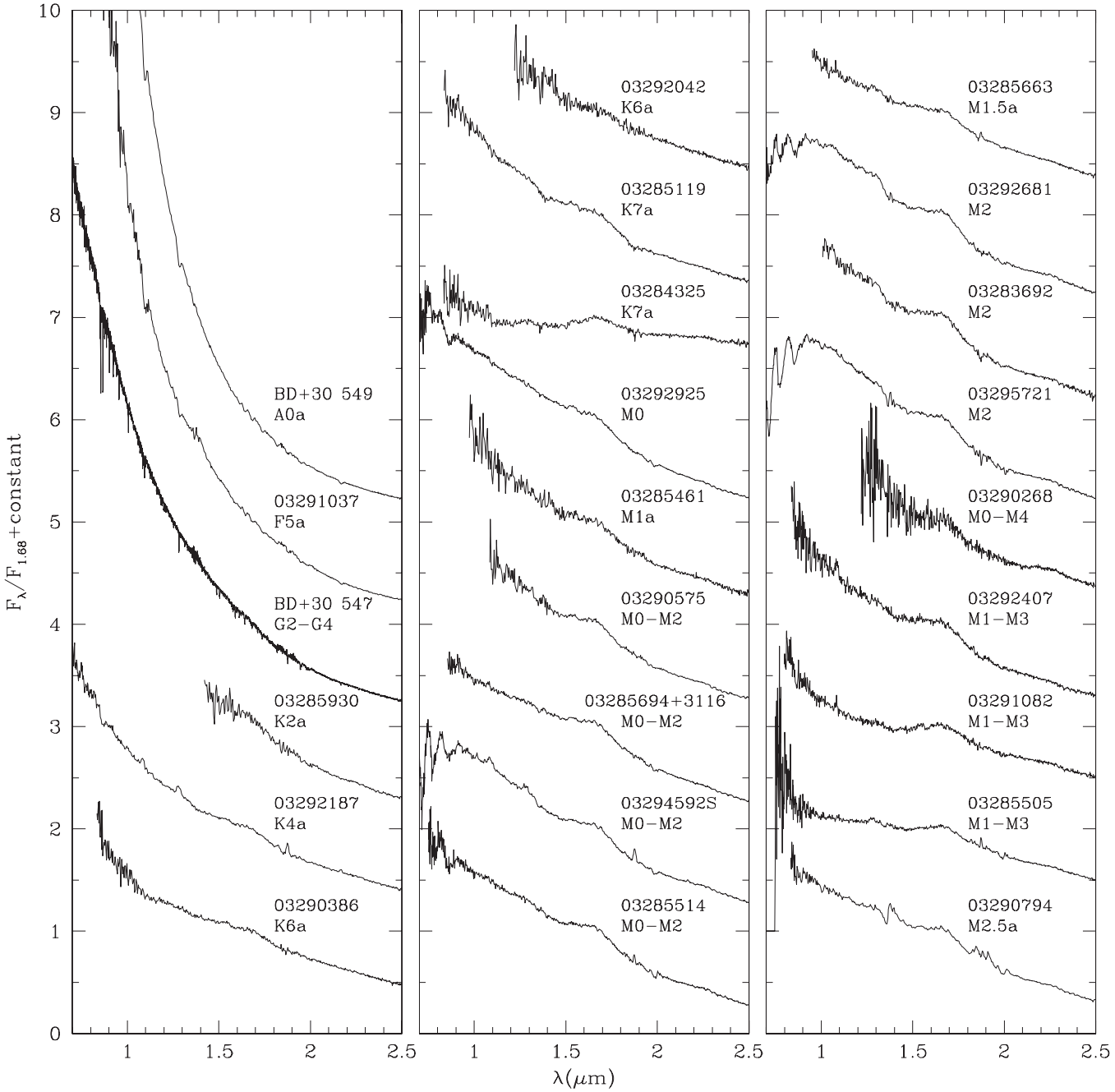

Figure 12. Near-IR spectra of members of NGC 1333. It was not possible to measure accurate spectral types from some of these data. Those spectra are labeled with the types that we have adopted from previous studies (denoted by a suffix of "a"). The remaining types have been measured from these spectra. The spectra have been dereddened to match the slopes of standards near 1 μm. The spectrum of BD+30°547 has a resolution of $R = 750$ while the other data have $R = 150$. Except for BD +30°547, each spectrum is labeled with the portion of the source name from Table 2 that corresponds to right ascension. For one object, additional digits of declination are listed to uniquely identify it among the members.

(The data used to create this figure are available.)

background dwarfs. Therefore, we treat them as members of IC 348. The stars may have been ejected from the cluster through dynamical interactions with other members (Kroupa 1998; Weidner et al. 2011).

IC 348 IRS J03442484+3213482. It was identified as a candidate protostar by Evans et al. (2009) and Young et al. (2015; source 405 in those studies). Its near-IR spectrum from SpeX is featureless. Protostars can have featureless spectra if significant veiling is present. However, such spectra are normally very red (see Figure 11), whereas the spectrum of this object is much bluer ($H - K_s \sim 0.5$). In addition, it is far from the area in the southern part of the cluster where most of the known protostars are found. As a result, we conclude that it is more likely to be a galaxy than a protostar, and we classify it as a non-member for the purposes of this work.

BD+30°547. Preibisch (1997) described it as a likely foreground star, but its proper motion is consistent with membership in NGC 1333 (E. Mamajek 2016, private

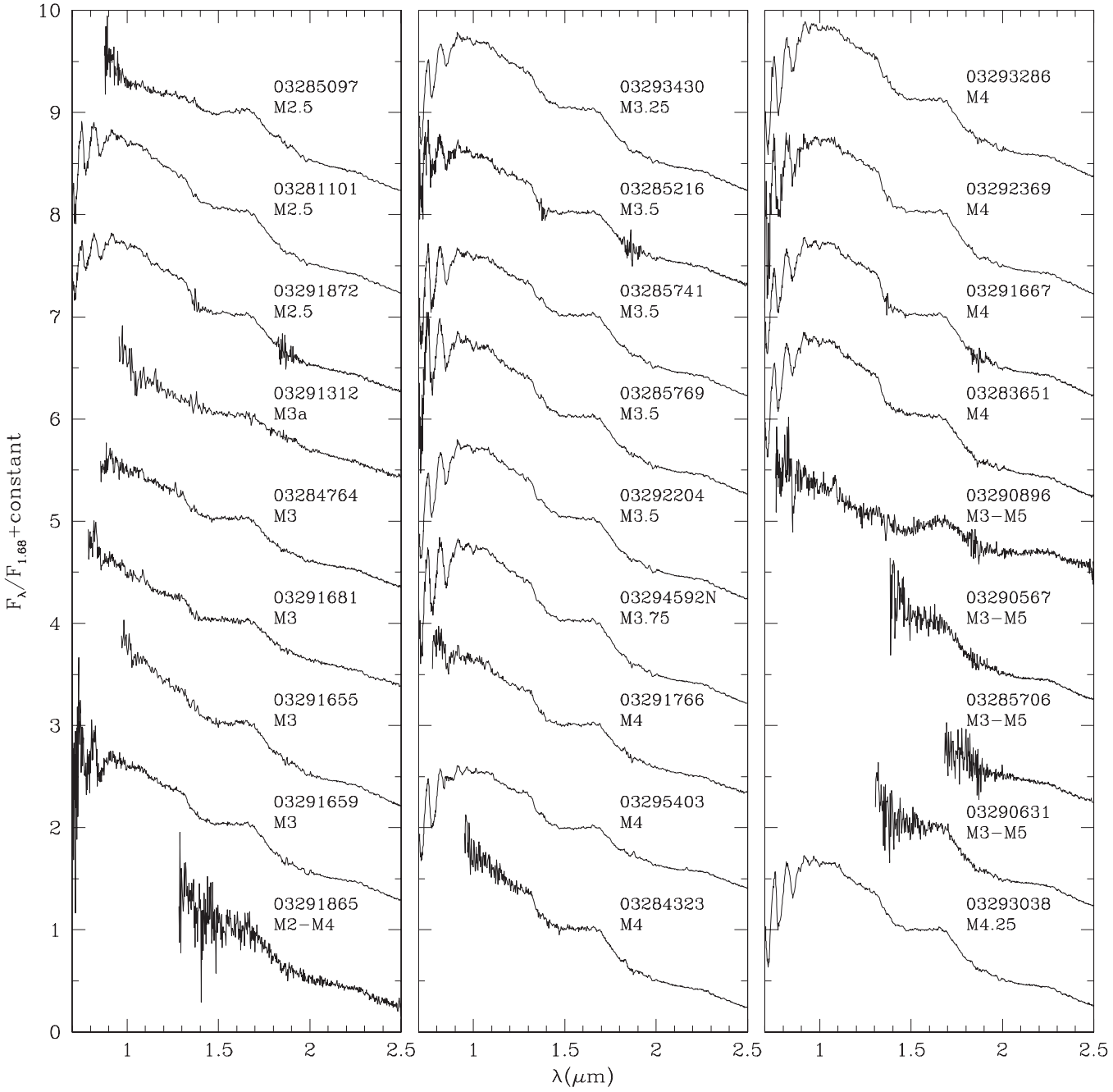

Figure 13. More near-IR spectra of members of NGC 1333 (see Figure 12). (The data used to create this figure are available.)

communication) and it exhibits X-ray emission. Some previous studies have concluded that it has IR excess emission at 24 μm (Evans et al. 2009; Rebull et al. 2015; Young et al. 2015), but that appears to be due to contamination from a protostar at a separation of 3.″4.

2MASS J03290575+3116396. Our SpeX type (M0–M2) is much later than previous types (late-G, A3).

[SVS76] NGC 1333 7. It has been classified as an early B giant through optical spectroscopy (Turnshek et al. 1980). Meanwhile, several studies have reported IR excess emission for this star based on images from *Spitzer*. However, it is detected with only low S/N at 8 μm and is not detected at 24 μm because of bright extended emission. Among the bands at shorter wavelengths where better photometry is available, only the [5.8] band exhibits a significant excess. Given the excess in that band and its location near the center of the cluster, the star is a promising candidate member, but we exclude it from our census of confirmed members because of the uncertainty in its spectral classification.

NGC 1333 IRS J03290347+3116179. It has a red, featureless near-IR spectrum. It is too close to a brighter star (2MASS J03290375+3116039) to be detected by *Spitzer* at >5 μm, but its

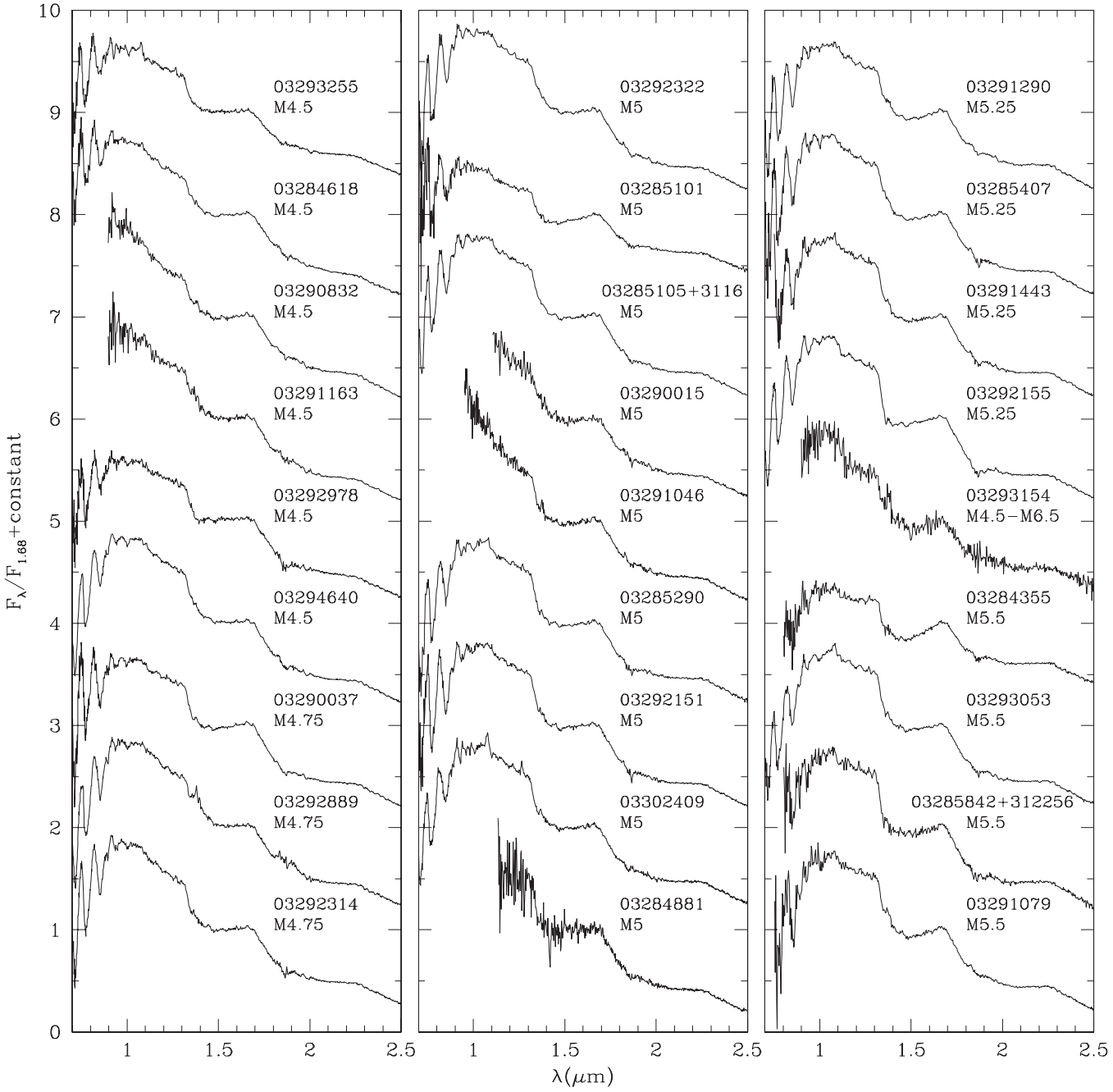

Figure 14. More near-IR spectra of members of NGC 1333 (see Figure 12).
(The data used to create this figure are available.)

[3.6]–[4.5] color is indicative of a protostar (Rebull et al. 2015), which would be consistent with the appearance of its spectrum. Its membership is further supported by its detection in X-rays and its close proximity to known members of the cluster.

2MASS J03290895+3122562. Its near-IR spectrum is red and featureless, which is consistent with the protostellar nature implied by its IRAC colors (Gutermuth et al. 2008; Evans et al. 2009).

2MASS J03294415+3119478. The strength of the steam bands for this object imply a type of M7–M8, but the overall slope of the SpeX data does not agree with that of any reddened standard. In addition, it is fainter than most members near its type in color–magnitude diagrams. With these characteristics, it is similar to 2MASS J04381486+2611399, which is a low-mass member of Taurus that is seen in scattered light from an edge-on disk (Luhman et al. 2007).

2MASS J03283695+3123121. Preibisch (1997) suggested that it is a foreground star based on its proper motion from Herbig & Jones (1983), but the motion that we have measured with IRAC is consistent with membership in NGC 1333.

NGC 1333 IRS J03284883+3117537. The S/N of our spectrum of this object is too low for classification. It is a candidate member based on its location on color–magnitude diagrams, proper motion, and excesses in the IRAC bands. It

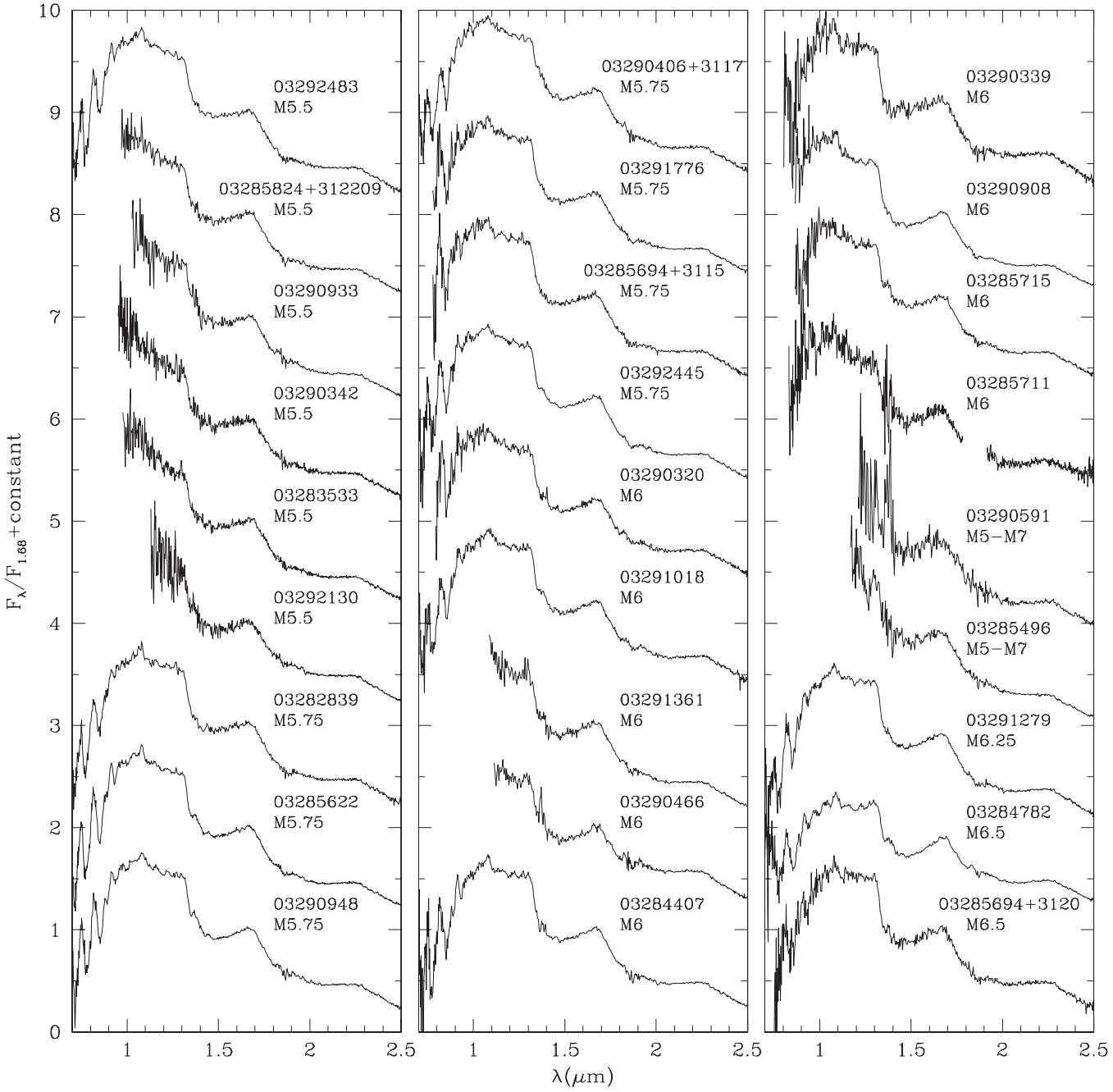

Figure 15. More near-IR spectra of members of NGC 1333 (see Figure 12). (The data used to create this figure are available.)

also may be detected at low S/N at 24 μm in images from MIPS, which would further support the presence of excess emission. It is included in our sample of remaining candidate members that lack classifications (Section 5.1).

2MASS 03302246+3132403. Evans et al. (2009) and Young et al. (2015) identified it as a possible protostar based on its mid-IR excess emission. However, it is detected in the optical bands of the Digitized Sky Survey, whereas most protostars are too heavily reddened for detections in those data. In addition, it is not near known protostars or high column densities of gas. Therefore, we conclude that it is probably a galaxy.

5. ANALYSIS OF NEW CENSUS

5.1. Completeness

As discussed in Section 3.1, we have focused our survey for members of IC 348 and NGC 1333 within a radius of 14′ from BD+31°643 in the former and within the ACIS-I images of the latter, which cover a field with a size of 18′ × 18′ (see Figure 1). To characterize the completeness of our new census for each field, we use a color–magnitude diagram in two bands that can detect objects at both low masses and high extinctions. Given the available data, the best options for these bands are H and K_s. In Figure 19, we plot diagrams of K_s versus $H - K_s$ for

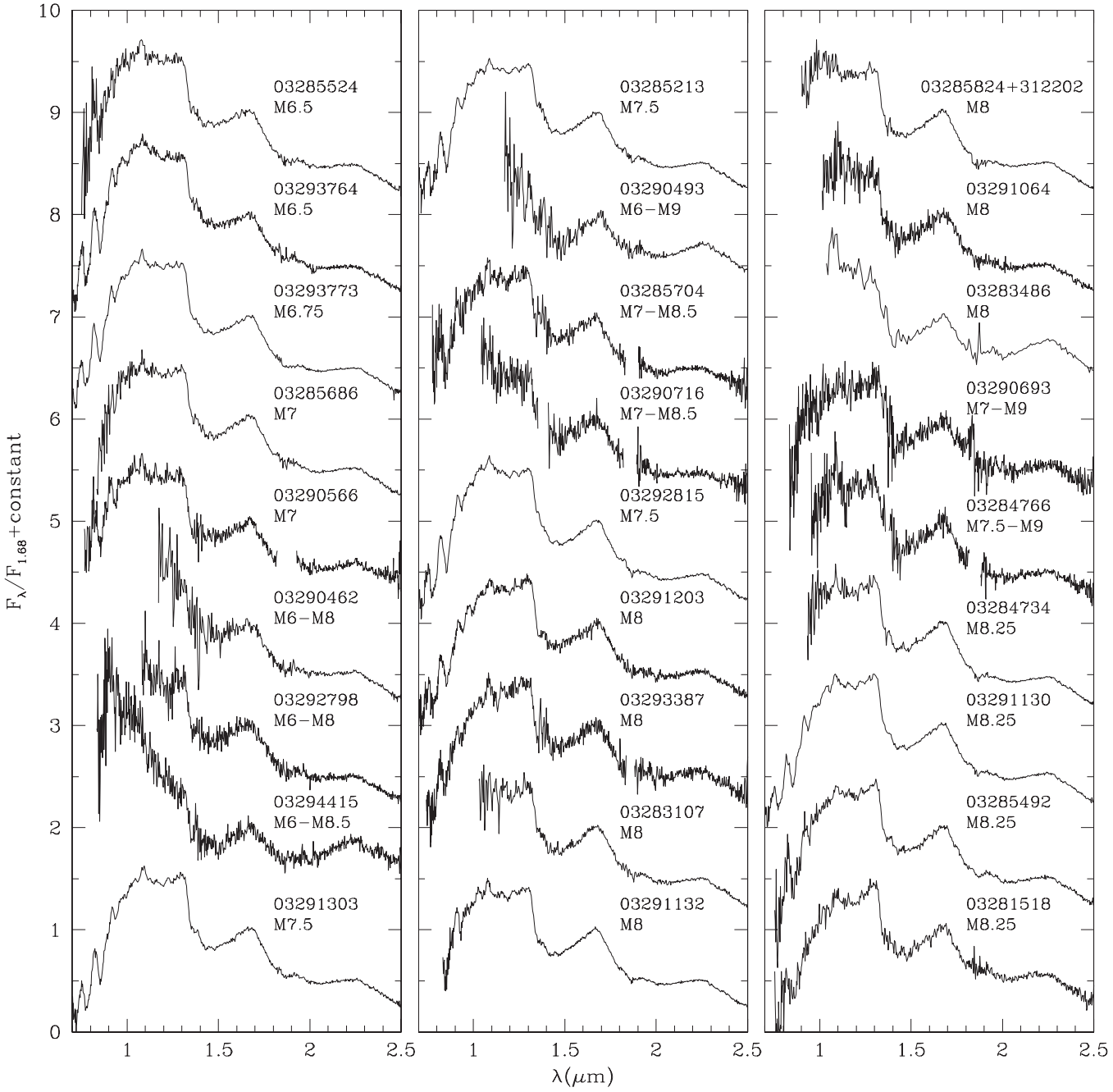

Figure 16. More near-IR spectra of members of NGC 1333 (see Figure 12).
(The data used to create this figure are available.)

all known members of IC 348 and NGC 1333, the remaining candidate members identified in Section 3 that lack spectra and are within the survey fields, and all other objects within those fields that are detected in H and K_s and that are not rejected as field stars by any of the color–magnitude diagrams that we used in selecting candidates. Thirteen and 20 members of IC 348 and NGC 1333, respectively, are absent from those diagrams, which consist of companions that are unresolved from brighter stars and protostars that are extended[5] or are not detected in H or K_s. In Figure 19, there are few remaining objects in the survey fields with undetermined membership status down to rather faint magnitudes for low-to-moderate levels of extinction. Specifically, our census appears to be nearly complete for extinction-corrected magnitudes of $K_s < 16.8$, 15.8, and 15.3 in the IC 348 field and for $K_s < 17.3$, 16.2, and 15.3 in the NGC 1333 field for $A_J < 1.5$, 3, and 5, respectively.

We can use our new census of IC 348 and NGC 1333 to examine the completeness of previous surveys for members. Luhman et al. (2003b) estimated that their census of a 16′ 14′ field in IC 348 was nearly complete for extinction-corrected magnitudes of $H < 15.5$ ($\lesssim$M8) for $A_V < 4$ ($A_J < 1.13$).

[5] Some of these protostars have measurements in the 2MASS Point Source Catalog, but are found to be dominated by extended emission in the higher resolution images from WIRCam.

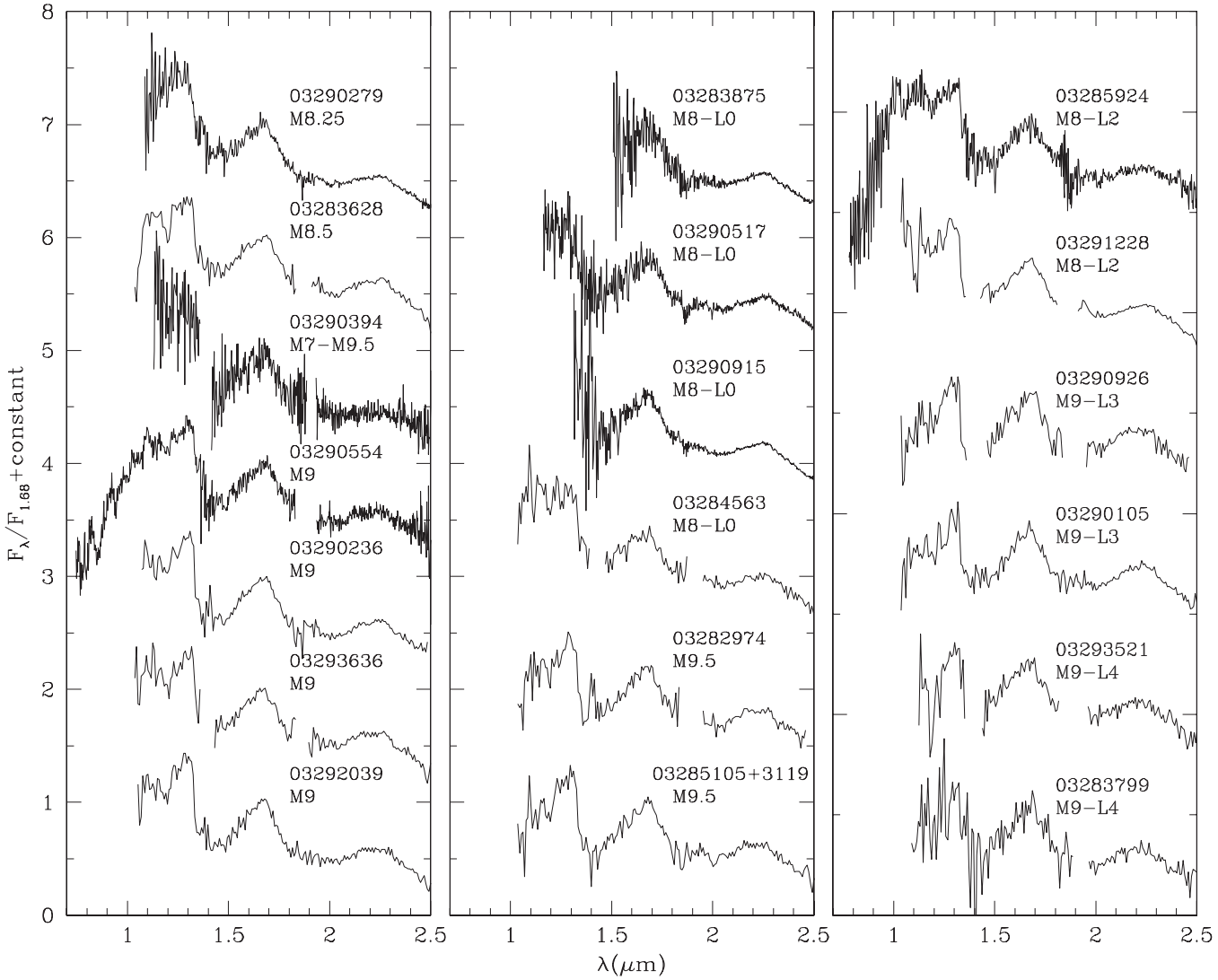

Figure 17. More near-IR spectra of members of NGC 1333 (see Figure 12).
(The data used to create this figure are available.)

Subsequent studies have not uncovered any additional members in their survey field and in that range of magnitudes and extinctions. Alves de Oliveira et al. (2013) noted that three of their new members were within the field from Luhman et al. (2003b). However, one of those objects, LRL 659, actually falls slightly outside of that field. The other two members, LRL 2050 and 22528 (M8 and M9), are fainter than the completeness limit from Luhman et al. (2003b). Meanwhile, Alves de Oliveira et al. (2013) concluded that their survey for brown dwarfs ($\gtrsim$M6.5) was complete down to ~0.013 $M_\odot$ ($\lesssim$M9) for $A_V \leqslant 4$ for a field that encompasses the entire cluster. However, we have found several new members at M6.5–M9 with $A_V < 4$, consisting of LRL 1254, LRL 1824, LRL 5103, LRL 10256, LRL 22185, LRL 22191, LRL 22317, and LRL 22778. Scholz et al. (2009, 2012a, 2012b) searched for members of NGC 1333 within a $30' \times 30'$ field covering the entire cluster using images that exhibited completeness limits of $J = 20.8$ and $K = 18$. We have identified 32 additional members above those limits (13 at $\leqslant$M6, 19 at $>$M6). The incompleteness in their census and the systematic offset between their spectral classification scheme and that applied to other regions like IC 348 (Section 4.2) cast doubt on the validity of the statements by Scholz et al. (2009, 2012a, 2012b, 2013) regarding the mass function in NGC 1333.

We also can characterize the fraction of members in our census that have been detected in X-rays by ACIS-I on *Chandra*. Stelzer et al. (2012) analyzed the four existing ACIS-I observations of IC 348, arriving at a list of 290 detected sources. They found X-ray counterparts for 187 of the 316 members from their adopted cluster census that were within the ACIS-I images. Using our updated census, 388 known members were observed by ACIS-I, 197 of which were detected. The members with X-ray detections can be identified in Table 1 via the presence of source designations from Stelzer et al. (2012). K. Getman (2016, in preparation) has performed a similar analysis for the existing ACIS-I data in NGC 1333. Among the 186 known members within those images, 98 have counterparts in their catalog of ACIS-I sources, as indicated in the column for evidence of membership in Table 2. In

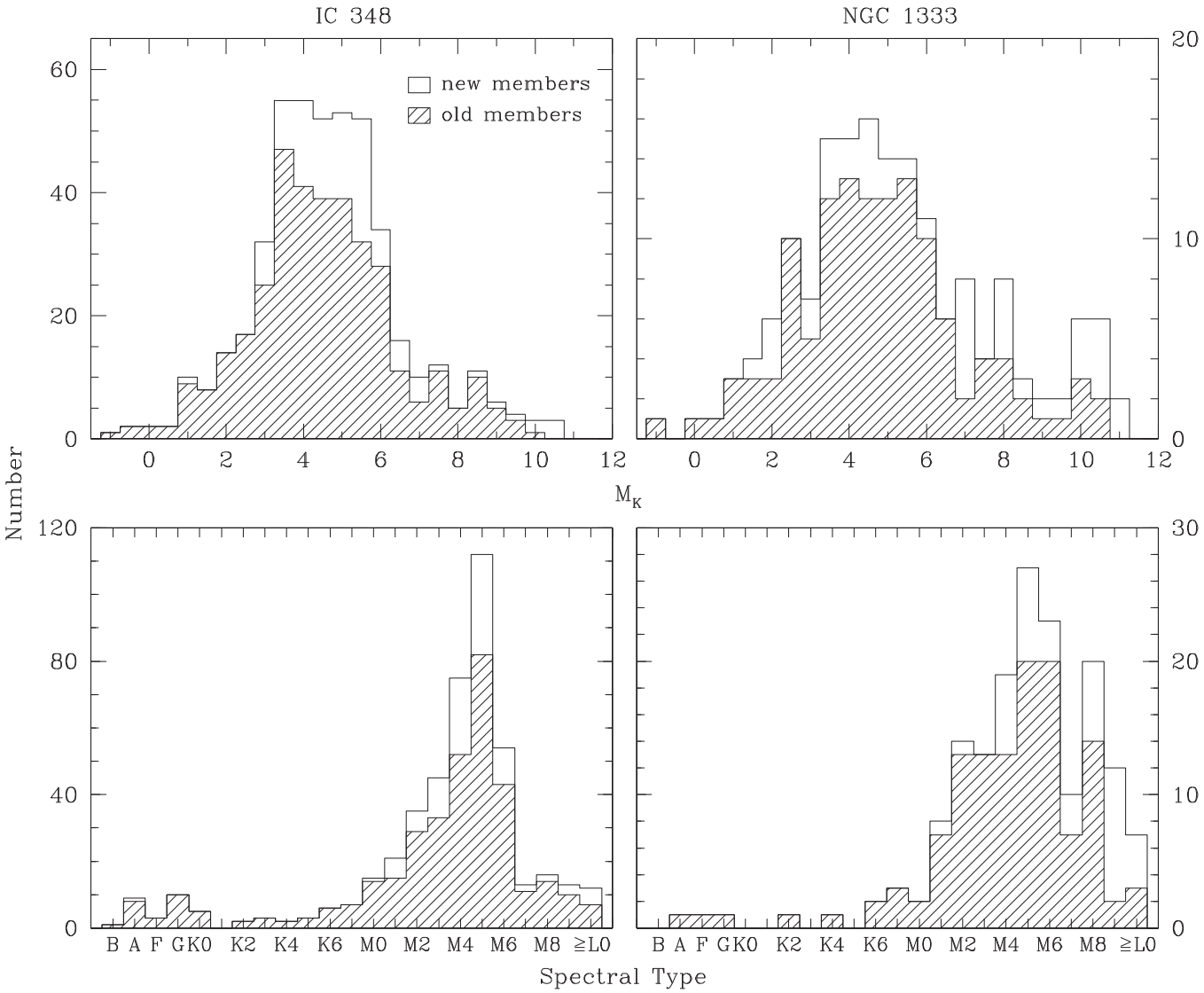

Figure 18. Distributions of spectral types and extinction-corrected M_K for previously known members of IC 348 and NGC 1333 (shaded histograms) and new members from this work (open histograms). Members that lack measured spectral types are absent, which consist of protostars with featureless spectra.

Figure 20, we plot the distributions of extinction-corrected M_K and spectral types for all known members of IC 348 and NGC 1333 within the ACIS-I images and for the members detected in those data. As expected, the fraction of members with X-ray detections decreases with fainter magnitudes and later spectral types, quickly approaching zero at $M_K > 6$ and >M7.

In Tables 4 and 5, we present our remaining candidate members that lack spectra and that are within the 14′ radius field in IC 348 and within the ACIS-I field in NGC 1333. Although it has been previously observed with spectroscopy, [SVS76] NGC 1333 7 is included with these candidates since its membership is uncertain (Section 4.4). The probability of membership varies substantially among these candidates. Those identified via both color–magnitude diagrams and proper motions are promising while those selected by proper motions alone (i.e., they lack the optical data needed for the color–magnitude diagrams) are much less likely to be members (Section 3.5). Based on their positions in the color–magnitude diagrams in Figure 19, most of the candidates should have spectral types of $\gtrsim$M6 if they are members. To check whether they have the near-IR colors expected for those types, we have included diagrams of $J - H$ versus $H - K_s$ for each cluster in Figure 19. Some of the candidates at $H - K_s < 1.5$ do resemble known late-type members in both $J - H$ and $H - K_s$, but most of the candidates at $H - K_s > 1.5$ have colors indicative of earlier types, and thus are likely to be background stars.

5.2. H–R Diagrams

We have constructed H–R diagrams for the known members of IC 348 and NGC 1333 in terms of M_K versus spectral type. We use absolute magnitude and spectral type instead of bolometric luminosity and effective temperature to avoid uncertainties in bolometric corrections and conversions between spectral type and temperature. We choose K_s for the band of the absolute magnitude because it is long enough in wavelength that extinctions are relatively low for most objects while short enough in wavelength that the fluxes are likely to be dominated by stellar photospheres rather than circumstellar disks. In addition, given the sensitivities of the available

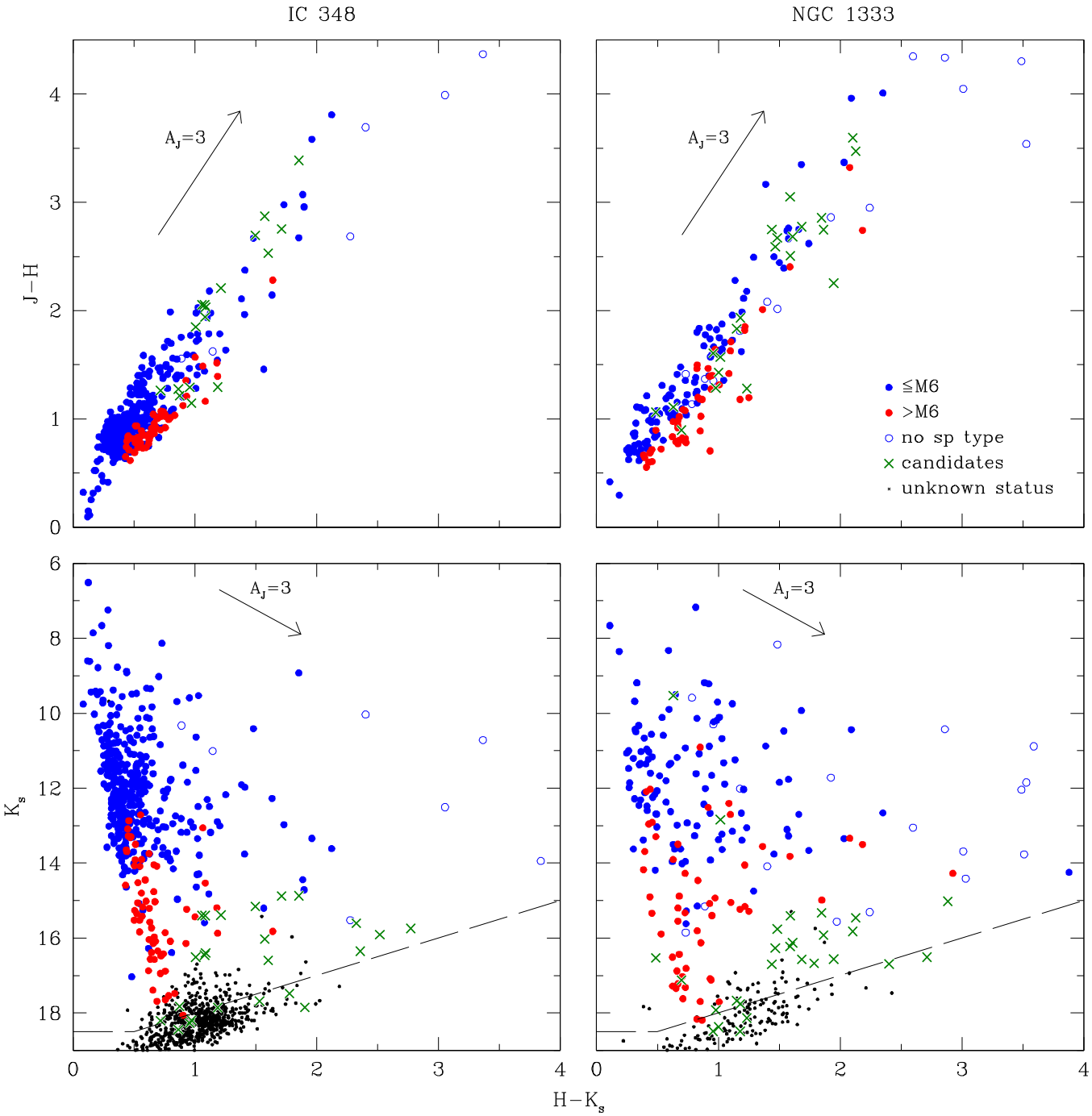

Figure 19. Near-IR color–color and color–magnitude diagrams for the known members of IC 348 and NGC 1333 (filled and open circles), candidate members within the 14′ radius field in IC 348 and within the ACIS-I field in NGC 1333 (crosses, Tables 4 and 5), and the remaining sources in those fields with unconstrained membership (small points; shown only in the bottom diagram). These data are from 2MASS, UKIDSS, WIRCam, and Muench et al. (2003). The completeness limits of the WIRCam images are indicated (long dashed lines).

images, those at K_s detect the largest fraction of the clusters members. The analysis in this section was also performed with the J and H bands, which produced identical results to those from K_s. We estimated extinctions for all known members of IC 348 and NGC 1333 that have measured spectral types in a similar manner as done by Furlan et al. (2011) for members of Taurus. For the members that we observed with IR spectroscopy, we have adopted the extinctions derived during the spectral classifications. For each of the remaining objects, we calculated the extinction from the excess in $J - H$ relative to the color expected for a young stellar photosphere at the spectral type in question (Luhman et al. 2010). After correcting the K_s measurements for extinction, we converted them to absolute magnitudes using distances of 300 pc for IC 348 (Herbst 2008) and 235 pc for NGC 1333 (Hirota et al. 2008). The resulting values of M_K are plotted as a function of spectral type in Figure 21. For comparison, we have included data for the members of the Upper Sco association compiled by Luhman & Mamajek (2012). We have adopted a distance of 145 pc for Upper Sco (Preibisch & Mamajek 2008) and have

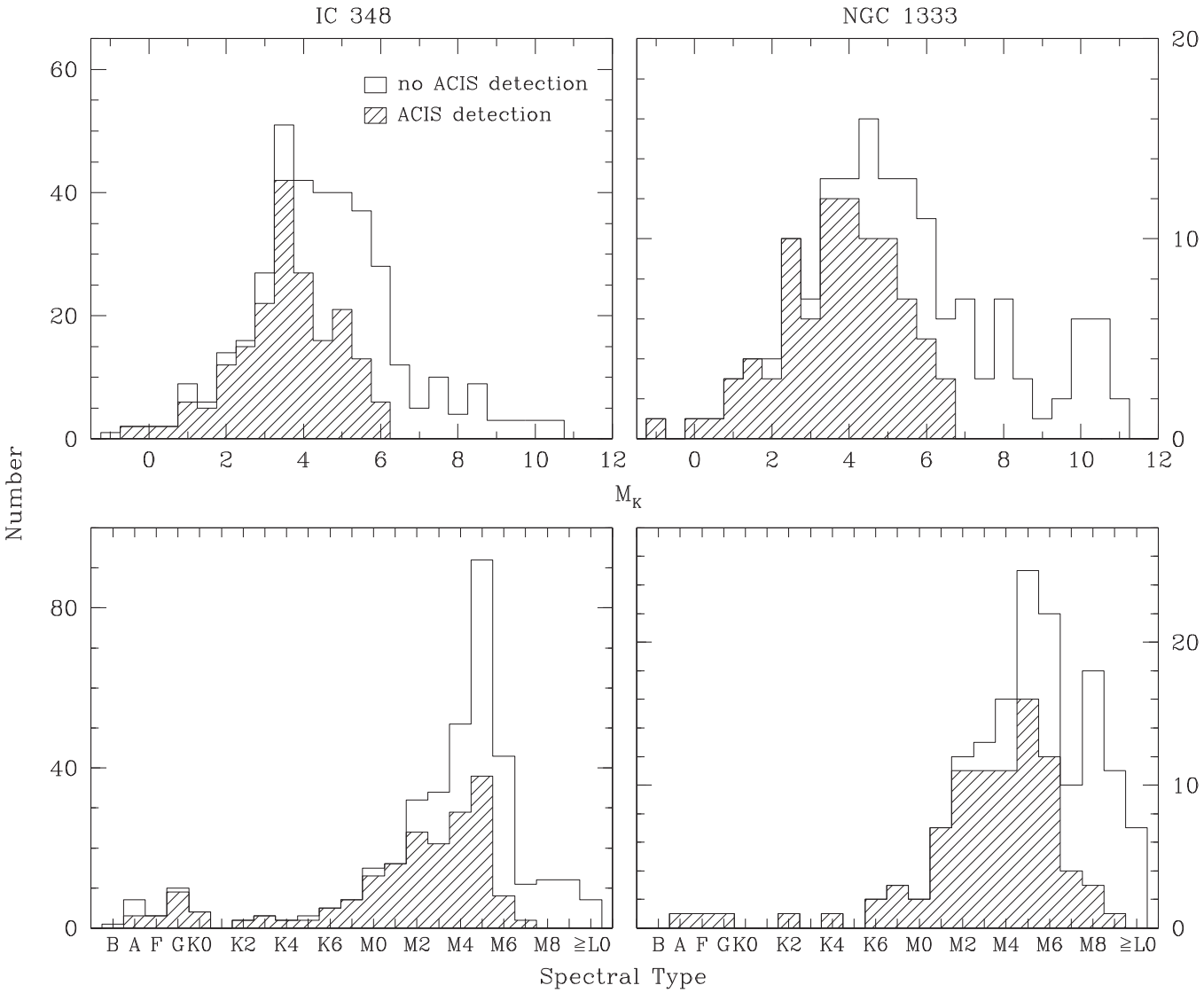

Figure 20. Distributions of spectral types and extinction-corrected M_K for members of IC 348 and NGC 1333 that are detected by ACIS-I on *Chandra* (shaded histograms) and that are within the ACIS-I fields but are not detected (open histograms, Preibisch & Zinnecker 2001, 2002; Getman et al. 2002; Winston et al. 2010; Forbrich et al. 2011; Stelzer et al. 2012, K. Getman 2016, in preparation).

estimated extinctions with the same methods that were applied to IC 348 and NGC 1333.

Several members of IC 348 and NGC 1333 are unusually faint for their spectral types, appearing below the cluster sequences in Figure 21. These objects include LRL 276, LRL 435, LRL 621, LRL 622, LRL 725, and LRL 4011 in IC 348 and sources 39, 92, 99, 110, and 122 from Gutermuth et al. (2008) in NGC 1333. The first five sources in IC 348 exhibited similar positions in the H–R diagram from Luhman et al. (2003b). As noted in Section 3.3, stars that are occulted by circumstellar disks often are observed primarily in scattered light, which results in underestimates of their luminosities. All of these stars do show evidence of disks in the form of mid-IR excess emission, so it is plausible that they are occulted by edge-on disks.

To compare the ages of IC 348, NGC 1333, and Upper Sco, we have computed the median values of M_K as a function of spectral type for each population. This was done by applying local linear quantile regression with the function `lprq` in the *quantreg* package (Koenker 2016) within R (R Core Team 2013) using a bandpass of one spectral type. The resulting median sequences are plotted together in Figure 21. We do not include the median for <M1 in NGC 1333 because of the small number of members at those types. The sequences for IC 348 and NGC 1333 are not offset vertically from each other, which would suggest that they have similar ages. However, NGC 1333 exhibits clear evidence of a younger age in the form of a greater abundance of protostars and circumstellar disks (Muench et al. 2007; Gutermuth et al. 2008, Section 5.4) and higher extinction (Figure 19). In order for the H–R diagram to produce a younger age for NGC 1333, we would need to adopt a larger distance for it (Herbig & Jones 1983) or a smaller distance for IC 348 (Ripepi et al. 2014), e.g., if the clusters have similar distances. Indeed, one would not expect the cluster distances to differ as much as we have assumed (65 pc) given that their projected separation is only ~17 pc, although it is possible that they reside in separate clouds along the line of site rather than a single cloud (Bally et al. 2008). Meanwhile, the median sequences for IC 348 (at 300 pc) and NGC 1333 (at 235 pc) are 0.4 mag

Table 4
Candidate Members of IC 348

Name[a]	LRL	Basis of Selection[b]	J[c] (mag)	H[c] (mag)	K_s[c] (mag)
IC 348 IRS J03434428+3203424	54299	pm	…	18.52 ± 0.04	15.74 ± 0.03
2MASS J03435901+3158282	1869	pm?	19.34 ± 0.03	16.59 ± 0.03	14.88 ± 0.03
IC 348 IRS J03440704+3159242	54486	pm?	…	19.21 ± 0.05	17.68 ± 0.03
IC 348 IRS J03441057+3157004	54502	pm?	20.47 ± 0.05	17.60 ± 0.03	16.03 ± 0.03
IC 348 IRS J03441387+3157170	54532	pm	20.73 ± 0.06	18.20 ± 0.03	16.60 ± 0.03
IC 348 IRS J03442154+3157381	52567	pm	18.81 ± 0.03	16.60 ± 0.03	15.39 ± 0.03
2MASS J03442217+3159371	10418	pm?	…	18.42 ± 0.03	15.90 ± 0.03
IC 348 IRS J03442355+3157339	1865	CMD, pm?	18.42 ± 0.03	16.48 ± 0.03	15.40 ± 0.03
IC 348 IRS J03442539+3207245	30053	CMD	20.58 ± 0.04	19.31 ± 0.04	18.44 ± 0.03
IC 348 IRS J03442750+3200477	22286	pm?	19.37 ± 0.03	17.52 ± 0.03	16.51 ± 0.03
IC 348 IRS J03442790+3157489	52620	pm	19.52 ± 0.03	17.48 ± 0.03	16.39 ± 0.03
2MASS J03442811+3158306	1886	pm?	20.11 ± 0.03	16.73 ± 0.03	14.87 ± 0.03
IC 348 IRS J03443171+3204326	30024	CMD	20.18 ± 0.03	18.92 ± 0.03	18.20 ± 0.03
IC 348 IRS J03443276+3158294	52641	pm	…	19.25 ± 0.04	17.48 ± 0.03
IC 348 IRS J03443516+3211052	596	CMD	19.91 ± 0.03	18.70 ± 0.03	17.82 ± 0.03
IC 348 IRS J03443537+3158233	52657	pm?	…	19.75 ± 0.10	17.85 ± 0.03
IC 348 IRS J03443631+3205066	30030	CMD	20.31 ± 0.03	19.16 ± 0.03	18.19 ± 0.03
2MASS J03444037+3157292	1929	pm	19.35 ± 0.03	16.65 ± 0.03	15.15 ± 0.03
IC 348 IRS J03444668+3201010	40172	pm	…	17.93 ± 0.03	15.61 ± 0.03
IC 348 IRS J03450146+3213418	30124	CMD	20.52 ± 0.05	19.23 ± 0.04	18.27 ± 0.03
IC 348 IRS J03450384+3200235	40182	pm	…	18.70 ± 0.04	16.35 ± 0.03
IC 348 IRS J03450403+3158129	22639	pm	20.33 ± 0.07	19.04 ± 0.05	17.85 ± 0.04
IC 348 IRS J03451226+3205502	22766	CMD, pm?	18.51 ± 0.03	16.46 ± 0.03	15.40 ± 0.03
IC 348 IRS J03451871+3205310	22898	pm?	19.59 ± 0.03	17.53 ± 0.03	16.45 ± 0.03

Notes.
[a] Coordinate-based identifications from the 2MASS Point Source Catalog when available. Otherwise, identifications are based on the coordinates measured from the WIRCam images in this work.
[b] Sources were selected as candidate members based on the color–magnitude diagrams in Figure 2 (CMD) or proper motions in Figure 4 (pm or pm?).
[c] WIRCam data from this work.

(This table is available in machine-readable form.)

brighter than the sequence for Upper Sco (at 145 pc), which corresponds to an age difference of 0.25 dex based on evolutionary models (e.g., Baraffe et al. 1998, 2015). If Upper Sco has an age of 11 Myr (Pecaut et al. 2012)[6], then IC 348 and NGC 1333 would have ages of 6 Myr. The latter agrees with the value derived for IC 348 by Bell et al. (2013) from color–magnitude diagrams and evolutionary models. However, a distance of 250 pc was adopted for IC 348 in that study. Using that distance, the sequences in Figure 21 would indicate similar ages for IC 348 and Upper Sco, which would be difficult to reconcile with the fact that IC 348 has higher abundances of disks and protostars and, unlike Upper Sco, is still associated with a molecular cloud. The *Gaia* mission (Perryman et al. 2001) should soon help isolate the sources of these discrepancies by providing accurate parallactic distances for IC 348, NGC 1333, and Upper Sco, as well as other nearby clusters and associations.

5.3. Initial Mass Functions

Previous studies have estimated the IMFs in IC 348 and NGC 1333 based on earlier samples of spectroscopically confirmed members (Luhman et al. 1998, 2003b; Greissl et al. 2007; Scholz et al. 2009, 2012a, 2012b; Alves de Oliveira et al. 2013).[7] Typically, the masses of individual objects were derived by combining estimates of bolometric luminosities and effective temperatures with the values predicted by evolutionary models. As a result, the IMFs depended on the adopted bolometric corrections, temperature scales, and models. To avoid those dependencies, we examine the IMFs in IC 348 and NGC 1333 in terms of observational parameters that should be roughly correlated with stellar mass, spectral type and extinction-corrected K_s. Note that these parameters still depend on the methods adopted for measuring spectral types and extinctions. As done in our previous studies of IMFs in star-forming regions, we attempt to construct a sample of members in each cluster that is representative and unbiased in terms of mass by considering all known members within a field and an extinction threshold for which the current census has a high level of completeness. Guided by the analysis of completeness in Section 5.1, we select extinction thresholds that are high enough to encompass large numbers of members while low enough that that the completeness extends to low masses, arriving at $A_J < 1.5$ for the 14′ radius field in IC 348 and $A_J < 3$ for the ACIS-I field in NGC 1333. In Section 5.1, we found that the census of IC 348 and NGC 1333 within these fields and extinction limits should be nearly complete for extinction-corrected magnitudes of $K_s < 16.8$ and 16.2,

[6] A younger age of 4–5 Myr has also been proposed for Upper Sco based on its low-mass stars (de Geus et al. 1989; Preibisch et al. 2002; Slesnick et al. 2006; Herczeg & Hillenbrand 2015).

[7] The IMFs in these clusters also have been constrained via IR luminosity functions (Lada & Lada 1995; Lada et al. 1996; Muench et al. 2003)

Table 5
Candidate Members of NGC 1333

Column Label	Description
Name	Source name[a]
Aspin	Name from Aspin et al. (1994)
Lada	Name from Lada et al. (1996)
Wilking	Name from Wilking et al. (2004)
Gutermuth	Name from Gutermuth et al. (2008)
Oasa	Name from Oasa et al. (2008)
Evans	Name from Evans et al. (2009)
Winston	Name from Winston et al. (2010)
Rebull	Name from Rebull et al. (2015)
Selection	Basis of selection[b]
Jmag	J magnitude
e_Jmag	Error in Jmag
Hmag	H magnitude
e_Hmag	Error in Hmag
Ksmag	K_s magnitude
e_Ksmag	Error in Ksmag
JHKref	JHK references[c]

Notes.
[a] Coordinate-based identifications from the 2MASS Point Source Catalog when available. Otherwise, identifications are based on the coordinates measured from the WIRcam images in this work.
[b] Sources were selected as candidate members based on X-ray emission (X, Getman et al. 2002; Winston et al. 2010, K. Getman 2016, in preparation), mid-IR excess emission (IR, Gutermuth et al. 2008; Evans et al. 2009), the color–magnitude diagrams in Figure 3 (CMD), or proper motions in Figure 4 (pm or pm?).
[c] 2 = 2MASS Point Source Catalog; u = UKIDSS Data Release 10; w = WIRCam data from this work.

(This table is available in its entirety in machine-readable form.)

respectively. These samples contain 341 and 120 members, respectively, which correspond to 71% and 59% of the known members.

The distributions of spectral types and extinction-corrected M_K for our extinction-limited samples of members of IC 348 and NGC 1333 are plotted in Figure 22. Relative to IC 348, NGC 1333 exhibits a surplus of objects with late spectral types and faint magnitudes. For instance, $N(\geqslant \mathrm{M6.5})/N(<\mathrm{M6.5}) = 54/287 = 0.188^{+0.025}_{-0.02}$ and $42/78 = 0.538 \pm 0.056$ and $N(M_K \geqslant 6.5)/N(M_K < 6.5) = 50/291 = 0.172^{+0.025}_{-0.019}$ and $40/80 = 0.50^{+0.056}_{-0.054}$ for IC 348 and NGC 1333, respectively. There are multiple possible explanations for the differences in these ratios. They could reflect a variation in the IMF between the two clusters, although a significant variation would be surprising given that the clusters have similar stellar densities and environments, and indeed have arisen from the same cloud (or at least related clouds). Because most of the spectral types in NGC 1333 have been measured with IR spectra, and the resulting classifications tend to have larger uncertainties than the optical types that are more frequently available in IC 348, one would expect the distribution of spectral types to be somewhat broader in NGC 1333, which would result in a higher abundance of late spectral types. However, this effect would not explain the difference between the two clusters in their distributions of M_K. Another possibility is that the average extinctions of members of star-forming regions vary with stellar mass, in which case extinction-limited samples would not be representative of the stellar populations in those clusters. For instance, if members at lower masses tend to have less extinction in the most embedded clusters like NGC 1333, then an extinction-limited sample could capture most of the brown dwarfs but miss many of the stars. In a cluster like IC 348 that has dispersed more of its natal cloud, the dependence of extinction on stellar mass could be smaller, leading to a larger, more representative ratio of stars to brown dwarfs in an extinction-limited sample. This scenario could account for the differences in the extinction-limited samples for IC 348 and NGC 1333. Finally, we note that both samples contain several known members that are fainter than the completeness limits, and the degree of incompleteness beyond those limits may differ between the two samples, which could somewhat inflate the perceived abundance of low-mass objects in one cluster relative to the other. To determine whether these last two issues are responsible for the surplus of low-mass objects in the extinction-limited sample for NGC 1333 relative to the sample in IC 348, it will be necessary to obtain additional data (e.g., photometry, spectroscopy, proper motions) that can extend the completeness limits of the census to higher extinctions and lower masses in both clusters.

Our work has provided new constraints on the minimum masses of the IMFs in IC 348 and NGC 1333. In each cluster, members are present down to and below the completeness limits, and thus the minimum of the IMF has not been detected. The faintest known members have $M_K = 10.4$ and 11.2, which correspond to masses of ~0.004–0.006 and 0.003–0.005 $M_\odot$, respectively, for ages of 1–3 Myr according to the evolutionary models of Burrows et al. (1997) and Chabrier et al. (2000).

5.4. Disk Fractions

We can combine our census of IC 348 and NGC 1333 with the previous mid-IR imaging of these clusters to measure the fractions of members that have circumstellar disks. A disk is present in the first three stages of a young stellar object, which consist of classes 0 and I (protostar+disk+infalling envelope) and class II (star+disk, Lada & Wilking 1984; Lada 1987; André et al. 1993; Greene et al. 1994). A star that has fully cleared its primordial disk is in the class III stage. A disk fraction can be defined as either N(I+II)/N(II+III) or N(II)/N(II+III) (class 0 objects are rare enough that their contribution is usually negligible). Because the ages measured for young clusters (with H–R diagrams) often apply to the class II and III sources, we choose the latter definition, as done in Luhman et al. (2010). Since protostars normally have heavily veiled, featureless spectra (Figure 11), we can exclude them from our calculations of disk fractions by considering only members that have measured spectral types. Members of star-forming regions are often discovered based on mid-IR excess emission from disks. As a result, samples of members can be biased in favor of disks, making it difficult to measure disk fractions that are representative of the stellar populations. However, IC 348 and NGC 1333 have been thoroughly surveyed for members using a variety of methods, and we have shown that the current membership samples for the 14′ radius field in IC 348 and the ACIS-I field in NGC 1333 are nearly complete for a wide range of masses and extinctions (Section 5.1). We have assigned the presence or absence of mid-IR excess emission for each member based on the results of previous disk surveys in these clusters with *Spitzer* (Luhman et al. 2005a; Lada et al. 2006; Muench et al. 2007; Gutermuth et al. 2008; Currie & Kenyon 2009; Evans et al. 2009; Arnold et al. 2012; Rebull et al. 2015; Young et al. 2015). A few of the faintest brown

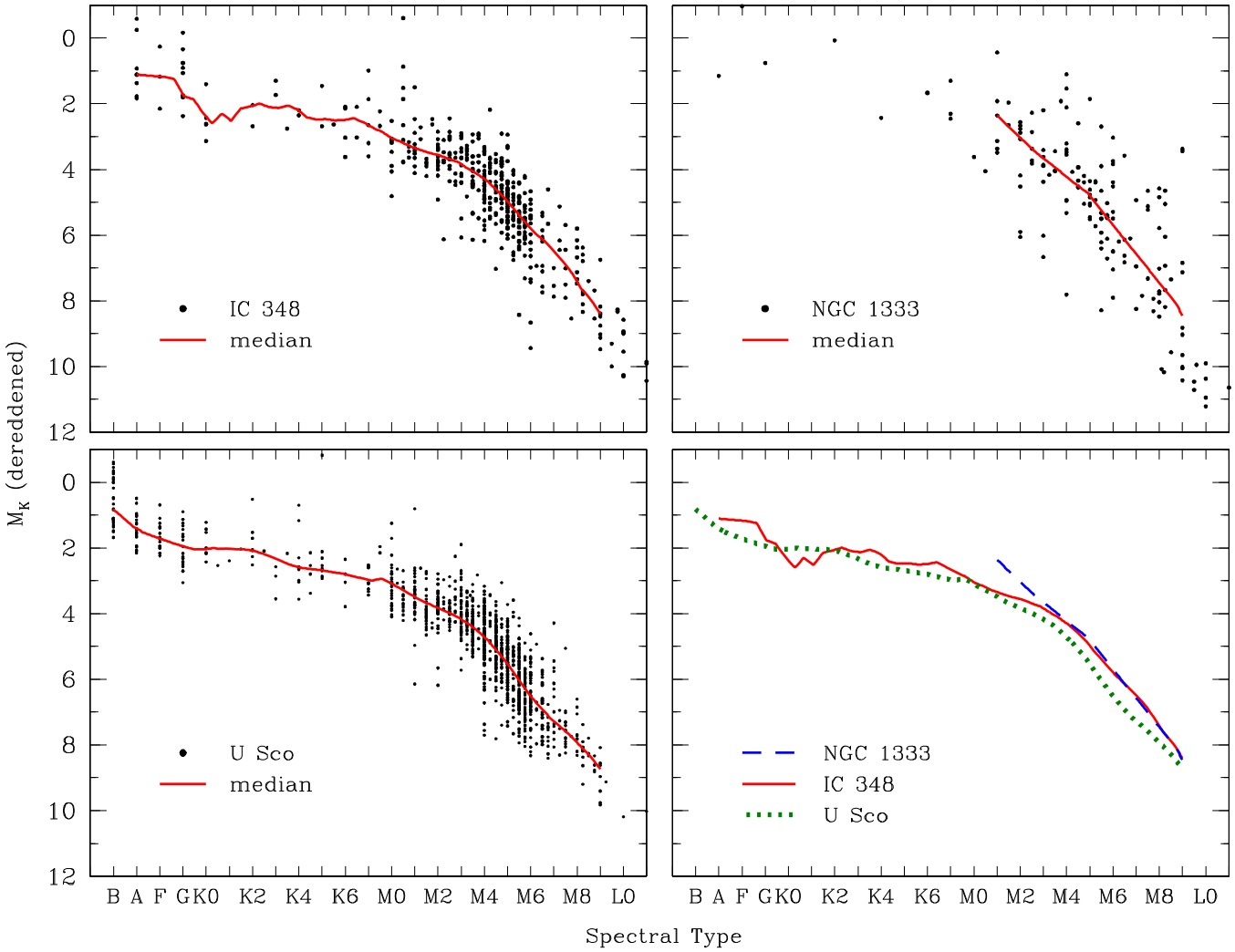

Figure 21. Top and left panels: extinction-corrected M_K vs. spectral type for the known members of IC 348, NGC 1333, and Upper Sco (points) assuming distances of 300, 235, and 145 pc, respectively. The median sequence is shown for each population (solid lines). Bottom right panel: the median sequences of IC 348 and NGC 1333 (solid and dashed lines) suggest that the clusters have similar ages. Those clusters are 0.4 mag brighter than Upper Sco (dotted line), corresponding to ages that are younger by 0.25 dex based on evolutionary models.

dwarfs lack sufficiently accurate photometry for determining whether excess emission in present; they are excluded from our calculations of disk fractions. In Table 6 and Figure 23, we list and plot the fraction of members that have excess emission as a function of spectral type for the 14′ radius field in IC 348 and for the ACIS-I field in NGC 1333. The latter has a higher disk fraction, which agrees with previous analysis of near-IR photometry (Lada & Lada 1995; Lada et al. 1996) and the *Spitzer* data (Lada et al. 2006; Muench et al. 2007; Gutermuth et al. 2008). The higher disk fraction in NGC 1333 is consistent with its higher abundance of protostars (Muench et al. 2007; Gutermuth et al. 2008) and the younger age implied by its greater obscuration. In each cluster, the disk fraction is roughly constant for the full range of spectral types.

5.5. Spatial Distributions

The spatial distributions of the stellar populations in IC 348 and NGC 1333 has been previously studied through analysis of probable members detected in near- and mid-IR imaging (Lada & Lada 1995; Lada et al. 1996; Muench et al. 2003; Gutermuth et al. 2008). The current census of each cluster now offers confirmation of membership, measurements of spectral types for most members, and a high level of completeness for most locations, masses, and extinctions. These features allow us to examine the spatial distributions of spectral types and offsets in M_K from the median cluster sequence at a given spectral type (ΔM_K), which serve as proxies for stellar masses and ages, respectively. We can also measure the spatial dependence of disk fractions using the mid-IR excess data compiled in the previous section. We define ΔM_K as M_K (median sequence at a star's spectral type) $-M_K$ (star), i.e., higher values of ΔM_K correspond to younger implied ages. We consider only members within the 14′ radius field in IC 348 and the ACIS-I field in NGC 1333 because of the well-defined completeness in those areas. The class 0 and I objects exhibit distinct spatial distributions compared to members in the more evolved classes, so we exclude them from our analysis by considering only members that have measured spectral types. We also omit members that are later than M9 since their types tend to have large uncertainties. For each of these samples of members, we have computed surface density as a function of position using

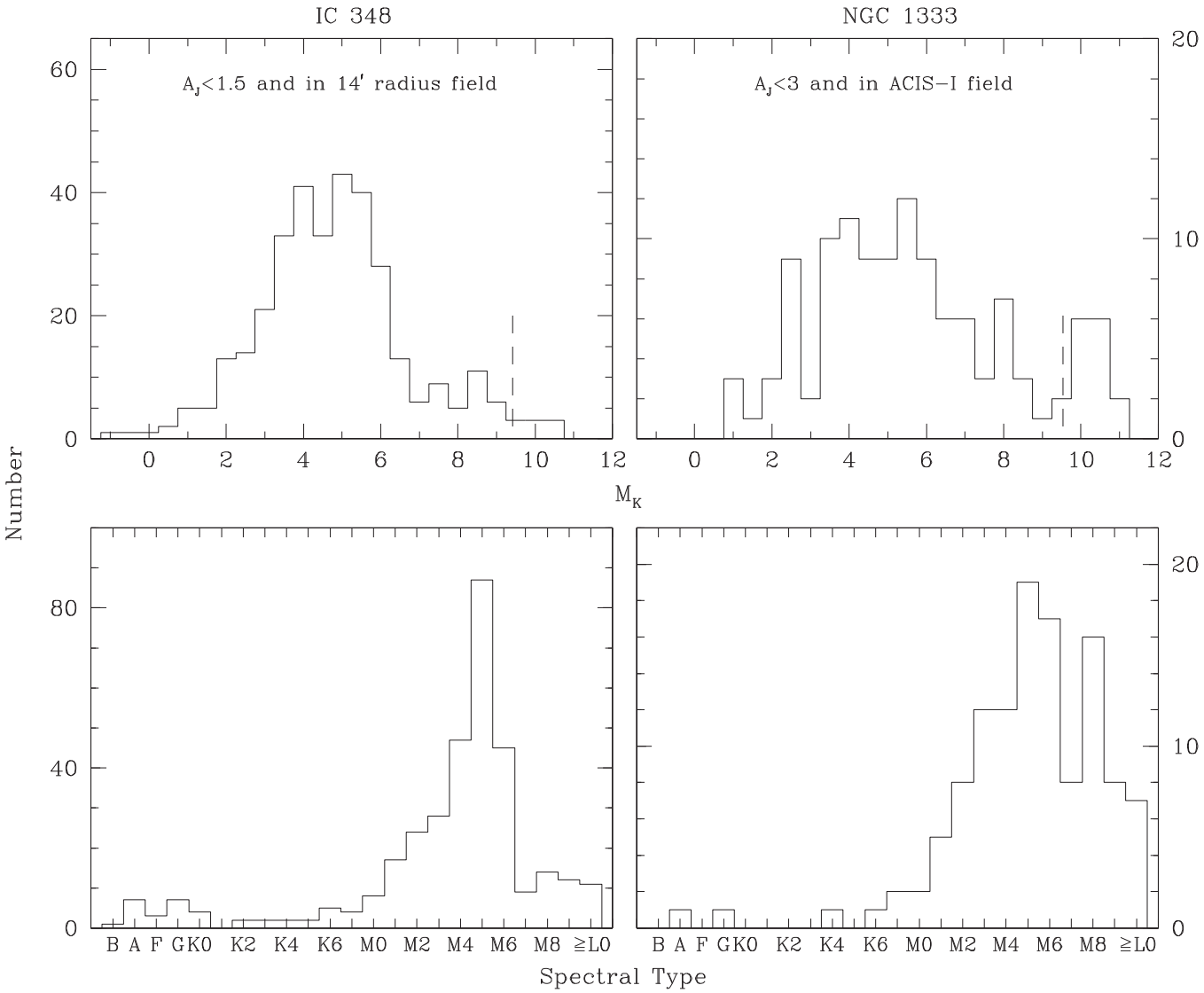

Figure 22. Distributions of spectral types and extinction-corrected M_K for members of IC 348 within its 14′ radius field that have $A_J < 1.5$ and members of NGC 1333 within the ACIS-I field that have $A_J < 3$. The dashed lines indicate the completeness limits of these samples of members for the fields and ranges of extinctions that they represent (see Figure 19).

Table 6
Disk Fractions in IC 348 and NGC 1333[a]

Spectral Type	IC 348	NGC 1333
<K6	$13/35 = 0.37^{+0.09}_{-0.07}$	$3/5 = 0.60^{+0.16}_{-0.21}$
K6–M3.5	$48/119 = 0.40^{+0.05}_{-0.04}$	$27/39 = 0.69^{+0.06}_{-0.08}$
M3.75–M5.75	$71/184 = 0.39^{+0.04}_{-0.03}$	$28/48 = 0.58 \pm 0.07$
M6–M8	$22/46 = 0.48 \pm 0.07$	$20/33 = 0.61^{+0.08}_{-0.09}$
>M8	$10/24 = 0.42^{+0.11}_{-0.09}$	$11/21 = 0.52 \pm 0.10$

Note.
[a] Fraction of sources with measured spectral types and within the 14′ radius field in IC 348 and within the ACIS-I field in NGC 1333 that exhibit mid-IR excess emission.

the `kde2d` function in the R package *MASS* (Venables & Ripley 2002), which performs a two-dimensional kernel density estimation with a bivariate normal kernel. We then identified the density contours that would divide the sample for a given cluster into three subsets that have equal numbers. We selected that number of sections to allow coarse measurements of the variations of median spectral type, ΔM_K, and disk fraction with surface density while also providing good number statistics within each section. The resulting contours are plotted in Figure 24 with the locations of all known members of each cluster. The average surface densities in these sections are 0.3, 1.0, and 3.0 arcmin^{-2} in IC 348 and 0.2, 0.9, and 2.6 arcmin^{-2} in NGC 1333. As found in previous studies, IC 348 is more centrally concentrated than NGC 1333, which exhibits a double cluster morphology (Lada et al. 1996).

For each of the three sections within IC 348 and NGC 1333 in Figure 24, we have computed the median spectral type, the median ΔM_K, and the disk fraction. The errors in the medians were estimated with bootstrapping. The resulting values are plotted for each section in Figure 25. None of these parameters exhibit significant variations among the sections in either cluster. Through analysis of the near-IR luminosity function of IC 348, Muench et al. (2003) found a higher abundance of

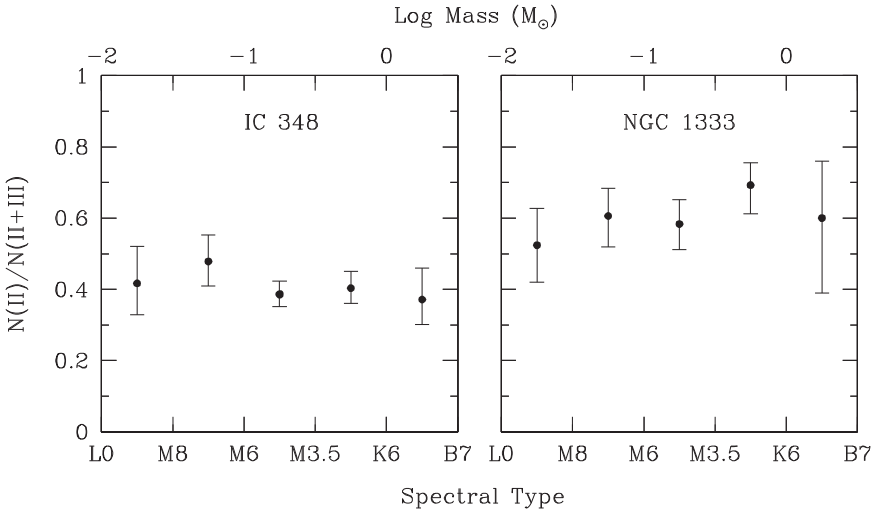

Figure 23. Fraction of sources with circumstellar disks (class II) as a function of spectral type within the 14′ radius field in IC 348 and within the ACIS-I field in NGC 1333 based on mid-IR photometry from *Spitzer* (Luhman et al. 2005a; Lada et al. 2006; Muench et al. 2007; Gutermuth et al. 2008; Currie & Kenyon 2009; Evans et al. 2009, Table 6). The boundaries of the spectral type bins have been chosen to correspond approximately to logarithmic intervals of mass.

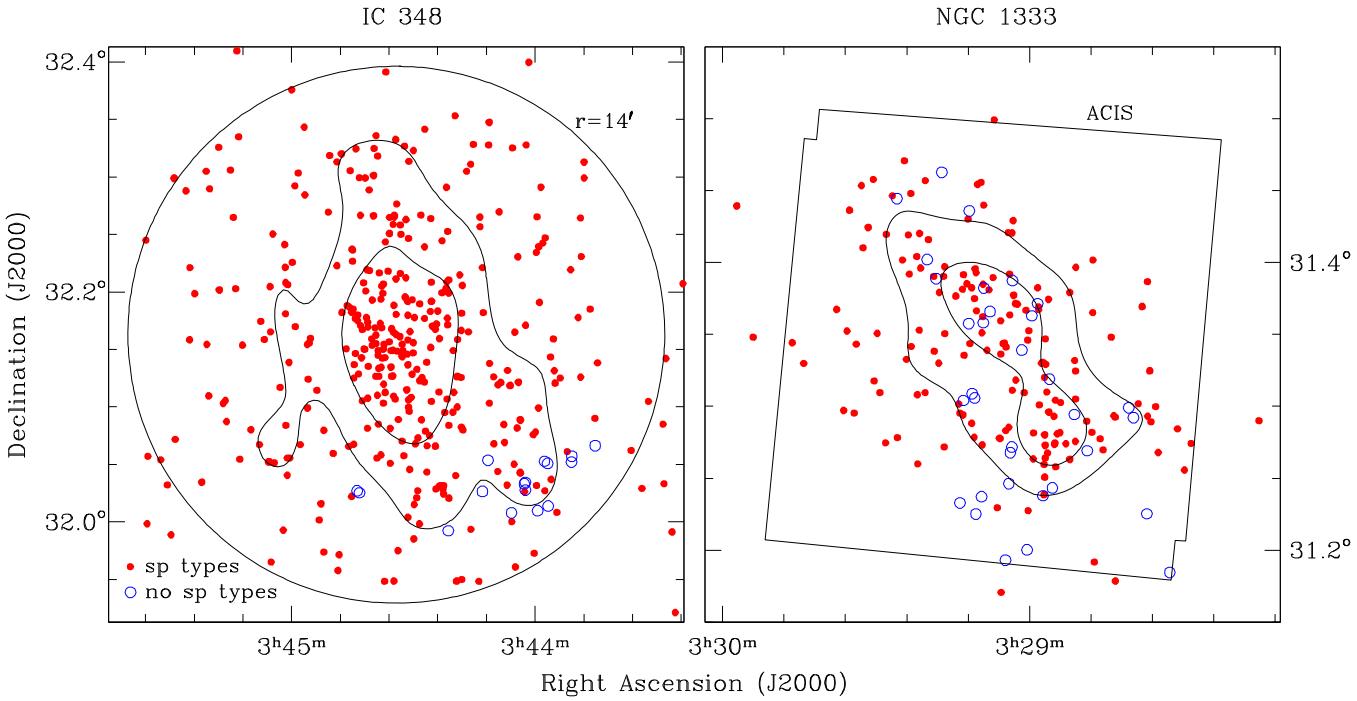

Figure 24. The positions of the known members of IC 348 and NGC 1333 that have measured spectral types (filled circles, ≈classes II and III) and those that do not (open circles, ≈classes 0 and I). The surface density of members with spectral types is represented by the contours. We have marked the 14′ radius field in IC 348 and the ACIS-I field in NGC 1333 within which we have focused our survey for members.

solar-mass stars in the core relative to the outskirts of the cluster. That surplus is also detected when distributions of spectral types are compared between the inner and outer portions of the cluster, although it is does not have a noticeable effect on the median types because low-mass stars are the dominant component of the stellar population throughout the cluster. Using X-ray and near-IR photometry, Getman et al. (2014) have detected age gradients in NGC 2024 and the Orion Nebula Cluster in which younger stars are found in the cores of the clusters. A trend of that kind is not present in the median values of ΔM_K for IC 348 and NGC 1333. For perspective, an age gradient like that reported for Orion (1.2–1.9 Myr) should correspond to a difference of 0.3 mag in M_K according to evolutionary models of low-mass stars. The errors in median ΔM_K are larger for NGC 1333 than for IC 348 because the former has a broader sequence at a given spectral type.

We note that a variety of more sophisticated methods are available for characterizing the spatial distributions of members of star-forming clusters (Gutermuth et al. 2009; Kuhn et al. 2014) and searching for evidence of mass segregation (Sagar et al. 1988; Hillenbrand & Hartmann 1998; Allison et al. 2009; Maschberger & Clarke 2011). The optimum approach for measuring the latter has been a subject of debate in recent years (Ascenso et al. 2009; Olczak et al. 2011; Parker & Goodwin 2015).

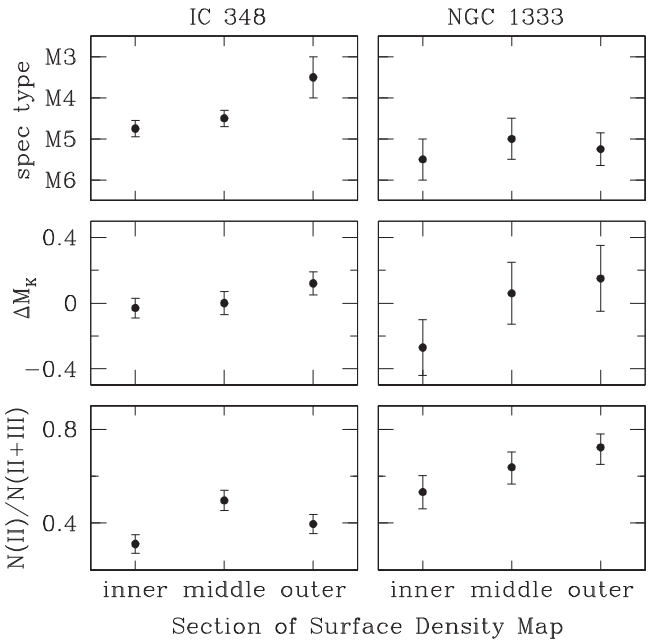

Figure 25. Median values of spectral type, ΔM_K, and disk fraction for members of IC 348 and NGC 1333 within the three regions of each cluster that are separated by the surface density contours in Figure 24. ΔM_K is defined as the difference in M_K between the median sequence of a cluster and an individual member in Figure 21 where positive values of ΔM_K correspond to positions above the median sequence (i.e., younger ages).

5.6. Candidate Binary Systems

Our census of IC 348 and NGC 1333 may contain resolved components of multiple systems. In Table 7, we have compiled all pairs of objects from our census that have separations less than 6″. We have omitted binaries that have been resolved only in high-resolution imaging and that lack spectral classifications of both components (Duchêne et al. 1999). For some of these pairs, both components have spectral types of late M, making them candidates for wide binary brown dwarfs (Luhman 2004; Luhman et al. 2009). The numbers of pairs are 23 and 8 for IC 348 and NGC 1333, respectively. To roughly estimate the fraction of these pairs that comprise binary systems, we performed a Monte Carlo simulation of the projected separations of unrelated cluster members using surface density maps of the known members. In ∼90% of the realizations, the number of chance alignments with separations of <6″ is between 5–15 for IC 348 and between 2–8 for NGC 1333. Thus, a significant fraction of the candidate binaries could consist of unrelated cluster members.

6. CONCLUSIONS

We have sought to improve the completeness of the census of stars and brown dwarfs in IC 348 and NGC 1333 and the accuracies of spectral types of known members of the latter. The results of this study are summarized as follows.

1. We have obtained optical and near-IR spectra of candidate members of IC 348 and NGC 1333 that have been selected based on X-ray emission, mid-IR excess emission, positions in color–magnitude diagrams, and proper motions. We have classified 100 and 42 of the candidates as new members of IC 348 and NGC 1333, respectively. The total numbers of known members are now 478 and 203. Two stars in IC 348, LRL 62 and LRL 155, have radial velocities that differ significantly from that of the bulk of the cluster, but they exhibit other evidence of membership, which suggests that they may have been ejected via dynamical interactions.
2. We have searched for new members primarily within a radius of 14′ from the B5 star BD+31°643 in IC 348 and within the area in NGC 1333 that was observed by ACIS-I on *Chandra* (18′ × 18′). These fields are large enough to encompass most or all members of the clusters. The new census is nearly complete for extinction-corrected magnitudes of $K_s < 16.8$, 15.8, and 15.3 in the IC 348 field and for $K_s < 17.3$, 16.2, and 15.3 in the NGC 1333 field for $A_J < 1.5$, 3, and 5, respectively. For perspective, $K_s = 15$ and 17 correspond to masses of ∼0.025 and 0.008 $M_\odot$, respectively, for an age of 3 Myr according to evolutionary models (Burrows et al. 1997; Chabrier et al. 2000; Baraffe et al. 2015). IC 348 and NGC 1333 now have two of the most complete membership lists among star-forming clusters.
3. The known members of IC 348 and NGC 1333 extend down to (and below) the completeness limits of the current census. As a result, we have not yet detected the low-mass cutoffs in the mass functions of these clusters. The faintest known members have $M_K = 10.4$ and 11.2, which imply masses of ∼0.004–0.006 and 0.003–0.005 $M_\odot$, respectively, for ages of 1–3 Myr based on evolutionary models.
4. In addition to the candidate members, we have performed spectroscopy on a large fraction (77%) of the previously known members of NGC 1333. These data provide greater uniformity in the spectral types among members of this cluster and relative to stars in other young clusters like IC 348.
5. To estimate the IMFs in IC 348 and NGC 1333, we have attempted to select a sample of members in each cluster that is unbiased in terms of mass. We have constructed extinction-limited samples for this purpose, which should have a high level of completeness down to low masses. The resulting sample for NGC 1333 has a higher abundance of low-mass objects than the sample for IC 348. For instance, $N(\geqslant\text{M6.5})/N(<\text{M6.5}) = 0.188^{+0.025}_{-0.02}$ in IC 348 and 0.538 ± 0.056 in NGC 1333. Similar fractions are found when the clusters are compared in terms of M_K. A variation in the IMF between the clusters would be surprising given their similar densities and environments. Instead, it is possible that average extinctions are lower for objects at lower masses, in which case extinction-limited samples may be biased in favor of low-mass objects in heavily embedded clusters like NGC 1333. To test that explanation, the completeness limits of the census of IC 348 and NGC 1333 need to be extended to higher extinctions.
6. We have constructed H–R diagrams for IC 348 and NGC 1333 in terms of spectral type and M_K. For the adopted distances of 300 and 235 pc, the median sequences of the clusters coincide, which suggests that they have similar ages. In contrast, NGC 1333 shows strong evidence of a younger age in the form of higher abundances of disk-bearing stars and protostars and greater obscuration. This discrepancy may indicate that IC 348 is closer or NGC 1333 is more distant than we

Table 7
Pairs of Members of IC 348 and NGC 1333 Separated by $<6''$

Name	Spectral Type	Name	Spectral Type	Separation (arcsec)
LRL 12 A	G0	LRL 12 B	A3	1.29
LRL 16	G6	LRL 33	M2.5	5.41
LRL 24 A	K6.5	LRL 24 B	M0	4.32
LRL 42 A	M4.25	LRL 42 B	M2.5	2.63
LRL 60 A	M2	LRL 60 B	M2	1.21
LRL 78 A	M0.5	LRL 78 B	M6.5	1.64
LRL 99 A	M3.75	LRL 99 B	M5.25	3.13
LRL 138	M4	LRL 3093	M5.5	2.80
LRL 160	M4.75	LRL 55400	…	5.65
LRL 165	M5.25	LRL 366	M5	5.65
LRL 166 A	M4.25	LRL 166 B	M5.75	0.79
LRL 187	M4.25	LRL 9187	M4.25	1.29
LRL 192	M4.5	LRL 1684	M5.75	4.74
LRL 210	M3.5	LRL 761	M7	4.51
LRL 259 A	M5	LRL 259 B	M5	2.08
LRL 1937	M0	LRL 1928	M5.5	4.35
LRL 233	M4.75	LRL 3171	L0	2.85
LRL 265	M3.25	LRL 148	M4	5.68
LRL 102	M0	LRL 22356	M3.75	1.90
LRL 104	M4	LRL 22317	M8.25	2.00
LRL 10148	M5	LRL 23177	M5.75	1.90
LRL 264	M3	LRL 4035	M5.5	2.56
LRL 54459	…	LRL 54460	…	5.54
2MASS J03284325+3117330	K7	2MASS J03284355+3117364	M5.5	5.06
2MASS J03285505+3116287	M2	2MASS J03285514+3116247	M1	4.24
2MASS J03285720+3114189	G3	NGC 1333 IRS J03285737+3114162	…	3.44
2MASS J03285769+3119481	M3.5	2MASS J03285741+3119505	M3.5	4.32
2MASS J03290279+3122172	M8.25	NGC 1333 IRS J03290236+3122159	M9	5.67
2MASS J03290493+3120385	M7.5	NGC 1333 IRS J03290517+3120370	M9	3.40
2MASS J03290575+3116396[a]	M1	NGC 1333 IRS J03290591+3116403	M6	2.14
2MASS J03294592+3104406S	M1	2MASS J03294592+3104406N	M3.75	2.77

Note.
[a] This star has an additional candidate companion, [OTS2008] 48, at a separation of $2''$.

have assumed. The *Gaia* mission should soon test this explanation by measuring parallactic distances for the clusters.

7. Based on mid-IR photometry, the fraction of members that have circumstellar disks is higher NGC 1333 than in IC 348 (N(II)/N(II+III) $\sim$ 0.6 and 0.4), which agrees with results for earlier samples of members. In each cluster, the disk fraction is roughly constant across the entire range of stellar masses (0.01–3 $M_{\odot}$).
8. For each cluster, we have examined the spatial distribution of stellar masses and ages by computing the median spectral types and median offsets in M_K from the median cluster sequence in three sections with differing stellar densities. We also have measured the disk fraction in each of these areas. None of these parameters exhibit significant variations with stellar density.

This work was supported by grant AST-1208239 from the NSF. We thank Konstantin Getman for providing his X-ray catalog of NGC 1333 and Catarina Alves de Oliveira for providing her near-IR spectra of candidate members of IC 348. We also thank Cameron Bell, Catarina Alves de Oliveira, Eric Feigelson, Konstantin Getman, Charles Lada, and Eric Mamajek for helpful discussions and comments on the manuscript. The IRTF is operated by the University of Hawaii under contract NNH14CK55B with NASA. The Gemini data were obtained through programs GN-2008B-Q-21, GN-2014B-Q-55, GN-2015B-Q-43, and GN-2015B-FT-10. Gemini Observatory is operated by AURA under a cooperative agreement with the NSF on behalf of the Gemini partnership: the NSF (United States), the NRC (Canada), CONICYT (Chile), the ARC (Australia), Ministério da Ciência, Tecnologia e Inovação (Brazil) and Ministerio de Ciencia, Tecnología e Innovación Productiva (Argentina). 2MASS is a joint project of the University of Massachusetts and IPAC at Caltech, funded by NASA and the NSF. This work used data from the NASA/IPAC Infrared Science Archive, operated by JPL under contract with NASA, and the SIMBAD database, operated at CDS, Strasbourg, France. The Digitized Sky Survey was produced at the Space Telescope Science Institute under U.S. Government grant NAG W-2166. The images of these surveys are based on photographic data obtained using the Oschin Schmidt Telescope on Palomar Mountain and the UK Schmidt Telescope. The plates were processed into the present compressed digital form with the permission of these institutions. WIRCam is a joint project of CFHT, Taiwan, Korea, Canada, and France. MegaCam is a joint project of CFHT and CEA/DAPNIA. CFHT is operated by the NRC of Canada, the Institute National des Sciences de l'Univers of the Centre National de la Recherche Scientifique of France, and the University of Hawaii. Subaru Telescope is operated by National Astronomical Observatory of Japan. The W.M. Keck Observatory is

operated as a scientific partnership among Caltech, the University of California, and NASA. The Observatory was made possible by the generous financial support of the W.M. Keck Foundation. The Center for Exoplanets and Habitable Worlds is supported by the Pennsylvania State University, the Eberly College of Science, and the Pennsylvania Space Grant Consortium.

REFERENCES

Allison, R. J., Goodwin, S. P., Parker, R. J., et al. 2009, MNRAS, 395, 1449
Alves de Oliveira, C., Moraux, E., Bouvier, J., et al. 2013, A&A, 549, A123
André, P., Ward-Thompson, D., & Barsony, M. 1993, ApJ, 406, 122
Arnold, L. A., Watson, D. M., Kim, K. H., et al. 2012, ApJS, 201, 12
Ascenso, J., Alves, J., & Lago, M. T. V. T. 2009, A&A, 495, 147
Aspin, C. 2003, AJ, 125, 1480
Aspin, C., Sandell, G., & Russell, A. P. G. 1994, A&AS, 106, 165
Bally, J., Walawender, J., Johnstone, D., Kirk, H., & Goodman, A. 2008, in Handbook of Star Forming Regions, Vol. 1, The Northern Sky, ed. B. Reipurth (San Francisco, CA: ASP), 308
Baraffe, I., Chabrier, G., Allard, F., & Hauschildt, P. H. 1998, A&A, 337, 403
Baraffe, I., Hormeier, D., Allard, F., & Chabrier, G. 2015, A&A, 577, 42
Bell, C. P. M., Naylor, T., Mayne, N. J., Jeffries, R. D., & Littlefair, S. P. 2013, MNRAS, 434, 806
Burgess, A. S. M., Moraux, E., Bouvier, J., et al. 2009, A&A, 508, 823
Burrows, A., Marley, M., Hubbard, W. B., et al. 1997, ApJ, 491, 856
Cardelli, J. A., Clayton, G. C., & Mathis, J. S. 1989, ApJ, 345, 245
Chabrier, G., Baraffe, I., Allard, F., & Hauschildt, P. 2000, ApJ, 542, 464
Cieza, L., Padgett, D. L., Stapelfeldt, K. R., et al. 2007, ApJ, 667, 308
Cieza, L. A., Schreiber, M. R., Romero, G. A., et al. 2012, ApJ, 750, 157
Cody, A. M., & Hillenbrand, L. A. 2014, ApJ, 796, 129
Cohen, M. 1980, AJ, 85, 29
Connelley, M. S., & Greene, T. P. 2010, AJ, 140, 1214
Cottaar, M., Covey, K. R., Foster, J. B., et al. 2015, ApJ, 807, 27
Currie, T., & Kenyon, S. J. 2009, AJ, 138, 703
Cushing, M. C., Rayner, J. T., & Vacca, W. D. 2005, ApJ, 623, 1115
Cushing, M. C., Vacca, W. D., & Rayner, J. T. 2004, PASP, 116, 362
de Geus, E. J., de Zeeuw, P. T., & Lub, J. 1989, A&A, 216, 44
Duchêne, G., Bouvier, J., & Simon, T. 1999, A&A, 343, 831
Elias, J. H., Joyce, R. R., Liang, M., et al. 2006, Proc. SPIE, 6269, 62694C
Esplin, T. L., & Luhman, K. L. 2016, AJ, 151, 9
Evans, N. J., II, Allen, L. E., Blake, G. A., et al. 2003, PASP, 115, 965
Evans, N. J., Dunham, M. M., Jørgensen, J. K., et al. 2009, ApJS, 181, 321
Fazio, G. G., Hora, J. L., Allen, L. E., et al. 2004, ApJS, 154, 10
Feigelson, E. D., Jackson, J. M., Mathieu, R. D., et al. 1987, AJ, 94, 1251
Flaherty, K. M., Muzerolle, J., Rieke, G. H., et al. 2012, ApJ, 748, 71
Flaherty, K. M., Muzerolle, J., Rieke, G. H., et al. 2013, AJ, 145, 66
Forbrich, J., Osten, R., & Wolk, S. J. 2011, ApJ, 736, 25
Foster, J. B., Cottaar, M., Covey, K. R., et al. 2015, ApJ, 799, 136
Fredrick, L. W. 1956, AJ, 61, 437
Furlan, E., Luhman, K. L., Espaillat, C., et al. 2011, ApJS, 195, 3
Getman, K. V., Feigelson, E. D., & Kuhn, M. A. 2014, ApJ, 787, 109
Getman, K. V., Feigelson, E. D., Townsley, L., et al. 2002, ApJ, 575, 354
Greene, T. P., Wilking, B. A., André, P., Young, E. T., & Lada, C. J. 1994, ApJ, 434, 614
Greissl, J., Meyer, M. R., Wilking, B. A., et al. 2007, AJ, 133, 1321
Gutermuth, R. A., Megeath, S. T., Myers, P. C., et al. 2009, ApJS, 184, 18
Gutermuth, R. A., Myers, P. C., Megeath, S. T., et al. 2008, ApJ, 674, 336
Harris, D. L., Morgan, W. W., & Roman, N. G. 1954, ApJ, 119, 622
Hatchell, J., & Dunham, M. M. 2009, A&A, 502, 139
Herbig, G. H. 1954, PASP, 66, 19
Herbig, G. H. 1998, ApJ, 497, 736
Herbig, G. H., & Jones, B. F. 1983, AJ, 88, 1040
Herbst, W. 2008, in Handbook of Star Forming Regions, Vol. 1, The Northern Sky, ed. B. Reipurth (San Francisco, CA: ASP), 372
Herczeg, G. J., & Hillenbrand, L. A. 2015, ApJ, 808, 23
Hillenbrand, L. A., & Hartmann, L. W. 1998, ApJ, 492, 540
Hirota, T., Bushimata, T., Choi, Y. K., et al. 2008, PASJ, 60, 37
Hodapp, K. W., Jensen, J. B., Irwin, E. M., et al. 2003, PASP, 115, 1388
Jørgensen, J. K., Harvey, P. M., Evans, N. J., II, et al. 2006, ApJ, 645, 1246
Jørgensen, J. K., Johnstone, D., Kirk, H., & Myers, P. C. 2007, ApJ, 656, 293
Koenker, R. 2016, quantreg: Quantile Regression. R package version 5.21, http://CRAN.R-project.org/package=quantreg
Kroupa, P. 1998, MNRAS, 298, 231
Kuhn, M. A., Feigelson, E. D., Getman, K. V., et al. 2014, ApJ, 787, 107
Lada, C. J. 1987, in IAU Symp. 115, Star Forming Regions, ed. M. Peimbert, & J. Jugaku (Dordrecht: Reidel), 1
Lada, C. J., Alves, J., & Lada, E. A. 1996, AJ, 111, 1964
Lada, C. J., Muench, A. A., Luhman, K. L., et al. 2006, AJ, 131, 1574
Lada, C. J., & Wilking, B. A. 1984, ApJ, 287, 610
Lada, E. A., & Lada, C. J. 1995, AJ, 109, 1682
Lawrence, A., Warren, S. J., Almaini, O., et al. 2007, MNRAS, 379, 1599
Lucas, P. W., Roche, P. F., Allard, F., & Hauschildt, P. H. 2001, MNRAS, 326, 695
Luhman, K. L. 1999, ApJ, 525, 466
Luhman, K. L. 2004, ApJ, 614, 398
Luhman, K. L., Adame, L., D'Alessio, P., et al. 2007, ApJ, 666, 1219
Luhman, K. L., Allen, P. R., Espaillat, C., Hartmann, L., & Calvet, N. 2010, ApJS, 186, 111
Luhman, K. L., Briceño, C., Stauffer, J. R., et al. 2003a, ApJ, 590, 348
Luhman, K. L., Lada, C. J., Hartmann, L., et al. 2005a, ApJL, 631, L69
Luhman, K. L., Lada, E. A., Muench, A. A., & Elston, R. J. 2005b, ApJ, 618, 810
Luhman, K. L., & Mamajek, E. E. 2012, ApJ, 758, 31
Luhman, K. L., Mamajek, E. E., Allen, P. R., Muench, A. A., & Finkbeiner, D. P. 2009, ApJ, 691, 1265
Luhman, K. L., McLeod, K. K., & Goldenson, N. 2005c, ApJ, 623, 1141
Luhman, K. L., Rieke, G. H., Lada, C. J., & Lada, E. A. 1998, ApJ, 508, 347
Luhman, K. L., Stauffer, J. R., Muench, A. A., et al. 2003b, ApJ, 593, 1093
Mainzer, A. K., & McLean, I. S. 2003, ApJ, 597, 555
Maschberger, T., & Clarke, C. J. 2011, MNRAS, 416, 541
Matthews, K., & Soifer, B. T. 1994, ExA, 3, 77
Merin, B., Brown, J. M., Oliveira, I., et al. 2010, ApJ, 718, 1200
Monet, D. G., Levine, S. E., Canzian, B., et al. 2003, AJ, 125, 984
Muench, A. A., Lada, C. J., Luhman, K. L., Muzerolle, J., & Young, E. 2007, AJ, 134, 411
Muench, A. A., Lada, E. A., Lada, C. J., et al. 2003, AJ, 125, 2029
Najita, J., Tiede, G. P., & Carr, J. S. 2000, ApJ, 541, 977
Oasa, Y., Tamura, M., Sunada, K., & Sugitani, K. 2008, AJ, 136, 1372
Olczak, O., Spurzem, R., & Henning, Th. 2011, A&A, 532, A119
Palau, A., Zapata, L. A., Rodriguez, L. F., et al. 2014, MNRAS, 444, 833
Parker, R. J., & Goodwin, S. P. 2015, MNRAS, 449, 3381
Pecaut, M. J., Mamajek, E. E., & Bubar, E. J. 2012, ApJ, 746, 154
Perryman, M. A. C., de Boer, K. S., Gilmore, G., et al. 2001, A&A, 369, 339
Preibisch, T. 1997, A&A, 324, 690
Preibisch, T. 2003, A&A, 401, 543
Preibisch, T., Brown, A. G. A., Bridges, T., Guenther, E., & Zinnecker, H. 2002, AJ, 124, 404
Preibisch, T., & Mamajek, E. 2008, in Handbook of Star Forming Regions, Vol. 2, The Southern Sky, ed. B. Reipurth (San Francisco, CA: ASP), 235
Preibisch, T., & Zinnecker, H. 2001, AJ, 122, 866
Preibisch, T., & Zinnecker, H. 2002, AJ, 123, 1613
Preibisch, T., & Zinnecker, H. 2004, A&A, 422, 1001
Preibisch, T., Zinnecker, H., & Herbig, G. H. 1996, A&A, 310, 456
R Core Team 2013, R Foundation for Statistical Computing, Vienna, Austria, www.R-project.org
Racine, R. 1968, AJ, 73, 233
Rayner, J. T., Cushing, M. C., & Vacca, W. D. 2009, ApJS, 185, 289
Rayner, J. T., Toomey, D. W., Onaka, P. M., et al. 2003, PASP, 115, 362
Rebull, L. M., Stapelfeldt, N. J., Evans, N. J., II, et al. 2007, ApJS, 171, 447
Rebull, L. M., Stauffer, J. R., Cody, A. M., et al. 2015, AJ, 150, 175
Rieke, G. H., Young, E. T., Engelbracht, C. W., et al. 2004, ApJS, 154, 25
Ripepi, V., Molinaro, R., Marconi, M., et al. 2014, MNRAS, 437, 906
Sagar, R., Miakutin, V. I., Piskunov, A. E., & Dluzhnevskaia, O. B. 1988, MNRAS, 234, 831
Schlafly, E. F., Green, G., Finkbeiner, D. P., et al. 2014, ApJ, 786, 29
Scholz, A., Geers, V., Clark, P., Jayawardhana, R., & Muzic, K. 2013, ApJ, 775, 138
Scholz, A., Geers, V., Jayawardhana, R., et al. 2009, ApJ, 702, 805
Scholz, A., Jayawardhana, R., Muzic, K., et al. 2012a, ApJ, 756, 24
Scholz, A., Muzic, K., Geers, V., et al. 2012b, ApJ, 744, 6
Scholz, R.-D., Brunzendor, J., Ivanov, G., et al. 1999, A&AS, 137, 305
Skrutskie, M., Cutri, R. M., Stiening, R., et al. 2006, AJ, 131, 1163
Slesnick, C. L., Carpenter, J. M., & Hillenbrand, L. A. 2006, AJ, 131, 3016
Stelzer, B., Preibisch, T., Alexander, F., et al. 2012, A&A, 537, 135
Straižys, V., Corbally, C. J., Kazlauskas, A., & Černis, K. 2002, BaltA, 11, 261
Strom, S. E., Grasdalen, G. L., & Strom, K. M. 1974a, ApJ, 191, 111
Strom, S. E., Strom, K. M., & Carrasco, L. 1974b, PASP, 86, 798

Strom, S. E., Vrba, F. J., & Strom, K. M. 1976, AJ, 81, 314
Turnshek, D. A., Turnshek, D. E., & Craine, E. R. 1980, AJ, 85, 1638
Vacca, W. D., Cushing, M. C., & Rayner, J. T. 2003, PASP, 115, 389
Venables, W. N., & Ripley, B. D. 2002, Modern Applied Statistics with S (4th ed.; New York: Springer)
Walawender, J., Bally, J., Franceso, J. D., Jørgensen, J., & Getman, K. 2008, in Handbook of Star Forming Regions, Vol. 1, The Northern Sky, ed. B. Reipurth (San Francisco CA: ASP), 346
Walawender, J., Bally, J., Kirk, H., et al. 2006, AJ, 132, 467
Walter, F. M., Brown, A., Mathieu, R. D., Myers, P. C., & Vrba, F. J. 1988, AJ, 96, 297
Weidner, C., Bonnell, I. A., & Moeckel, N. 2011, MNRAS, 410, 1861
Werner, M. W., Roellig, T. L., Low, F. J., et al. 2004, ApJS, 154, 1
Wilking, B. A., Meyer, M. R., Green, T. P., Mikhail, A., & Carlson, G. 2004, AJ, 127, 1131
Winston, E., Megeath, S. T., Wolk, S. J., et al. 2009, AJ, 137, 4777
Winston, E., Megeath, S. T., Wolk, S. J., et al. 2010, AJ, 140, 266
Young, K. E., Young, C. H., Lai, S.-P., Dunham, M. M., & Evans, N. J. 2015, AJ, 150, 40